

國立交通大學

資訊科學與工程研究所

碩士論文

結合三維定位與反光特性之表面最佳化技術



**Combine Stereo Positions and Reflectance Properties
for 3D Surface Optimization**

研究生：張文星

指導教授：林奕成 博士

中華民國九十六年七月

結合三維定位與反光特性之表面最佳化技術
Combine Stereo Positions and Reflectance Properties for 3D
Surface Optimization

研究生：張文星

Student : Wen-Xing Zang

指導教授：林奕成

Advisor : I-Chen Lin

國立交通大學
資訊科學與工程研究所
碩士論文



Submitted to Institute of Computer Science and Engineering
College of Computer Science

National Chiao Tung University

in partial Fulfillment of the Requirements

for the Degree of

Master

in

Computer Science

July 2006

Hsinchu, Taiwan, Republic of China

中華民國九十六年七月

結合三維定位與反光特性之表面最佳化技術

研究生:張文星

指導教授: 林奕成 博士

國立交通大學

資訊科學與工程研究所



本論文提出一個表面最佳化的演算法，當對真實的物體做重建動作且最佳化表面的同時亦可以取得其反射特性。我們使用結構光三維定位的系統去獲得一組較精確的起始三維模型。接著使用 Phong 和一個雙向次表面散射反射分配函數的模組來逼近真實場景的光反射特性。最後，在最佳化三維位置和光反射特性後，一組較精確的三維表面就可以被取得。不像大部份之前對於三維重建的方法，重建一些非只有散射特性或具次表面散射的材質物體是一個麻煩的問題。而且當我們重建了一組更精確的三維表面之餘，此物體的光反射特性我們亦取得，可以使用在描繪於虛擬場景時更真實且多變。

關鍵字: 結構光, 三維定位重建, Phong 模型, 雙向次表面散射反射函數, 共軛梯度法。

Combine Stereo Positions and Reflectance Properties for 3D Surface Optimization

Student: Wen-Xing Zhang

Advisor: Dr. I-Chen Lin

**Institute of Computer Science & Engineering
National Chiao Tung University**



This thesis presents an optimization algorithm to simultaneously estimate both the 3D shape and parameters of a surface reflectance model from real objects. We use stereo structured light system to obtain initial stereo positions. And the Phong and the BSSRDF reflectance model are used to approximate the surface reflectance. After optimizing both of the shape geometry and reflectance properties, a more accurate surface can be acquired. Unlike most previous work in shape reconstruction, the proposed method deals with the troublesome problem of scanning Non-Lambertian and subsurface-scattering objects. In addition to a more accurate surface, the reflectance parameters can also be used for advanced rendering.

Keyword: structured light, stereo reconstruction, Phong model, BSSRDF, conjugate gradient.

Acknowledgements

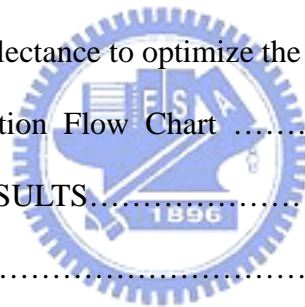
First of all, I would like to thank my advisor, Dr. I-Chen Lin, for his guidance in the past two years. Also, I appreciate all members of Computer Animation & Interactive Graphics Lab for their help and push. And last, I am grateful to my family for their support and encouragement.



Contents

摘要.....	i
ABSTRACT.....	ii
Acknowledge.....	iii
CONTENTS.....	iv
LIST OF FIGURES.....	vi
1. INTRODUCTION.....	1.
1.1 Background.....	1.
1.2 Motivation.....	2.
1.3 Purpose.....	3
1.4 Contribution.....	4
1.5 System Overview.....	4
1.6 Organization.....	5
2. RELATED WORK.....	6
2.1 Acquisition of 3D geometry.....	6
2.2 Light diffusion reflection model.....	9
2.3 Combining algorithms.....	11
3. ACQUISITION OF POSITION.....	14
3.1 Projector calibration.....	14
3.1.1 Cross-ratio.....	15
3.1.2 Calibration Box.....	16
3.1.3 Computing the strip planes.....	16
3.1.4 Adjust the normal on stripe plane.....	18
3.2 Coded Structured light.....	18

3.2.1	Binary coded and phase shifting.....	19
3.2.2	Single pattern sequence.....	20
3.3	Computing the image-to-world transformation.....	21
3.3.1	Estimating camera model.....	21
3.3.2	Estimating 3D positions.....	24
4.	RECONSTRUCTION AND OPTIMIZATION.....	26
4.1	Reflectance model.....	28
4.1.1	Phong model.....	28
4.1.2	BSSRDF model.....	29
4.2	Optimization.....	31
4.2.1	Using positions to improve reflectance.....	31
4.2.2	Using reflectance to optimize the positions.....	32
4.2.3	Optimization Flow Chart	33
5.	EXPERIMENT AND RESULTS.....	34
5.1	A Bunny.....	35
5.2	A marble statue.....	42
5.2.1	Stereo positions.....	42
5.2.2	Optimize result.....	44
6.	CONCLUSION AND FUTURE WORK.....	46
6.1	Conclusion.....	46
6.2	Future work.....	46
	REFERENCE.....	47



List of Figures

Fig.1 System overview.	5
Fig.2 (a), (b) Two images taken from one of the cameras. (c) Shaded rendering of the reconstructed model by window spacetime analysis.[6]	7
Fig.3 Reconstruction by examples. (a) Input data (one of 13 sets). (b) Views of the reconstructed model.[7]	7
Fig.4 (a) An ordinary photo. (b) Shape-from-shading applied to an object in the image to estimate its normals. (c) Pixel patches formed by clustering normals. (d) Texture synthesized on these patches and aligned with neighboring patches. (e) Final result with texture orientation distortion, displacement mapping and environment mapping.[8].....	8
Fig5. Clay horse. Left column: Images of the clay horse sequence. Right column: Similar view-points of the reconstructed model using graph-cuts.[14]	8
Fig6. (a) input image data. (b) result model.[4]	9
Fig.7 A simulation of subsurface scattering in a marble bust. The marble bust is illuminated from the back and rendered with: (a) the BRDF approximation (b) the BSSRDF approximation, and (c)a full Monte Carlo simulation. [3]	10
Fig.8 A multi-layered model of human skin using measured parameters for the individual skin layers[10]	11
Fig.9 least square optimization. (Left) Several range scans were aligned and merged. (Right) The result was later optimized with mapped normals coming from several independent photometric stereo scans.[1]	12
Fig. 10 1 nd row input images of a real mouse, down: 2 nd row. Optimized reflectance model with the initial shape. 3 rd row. Optimized results at the 1 st step. Optimized results at 2 st step.[2]	13
Fig.11 Projective calibration using 3 known non-coplanar sets of 3 collinear world points	

(dark circles $\{P_i, Q_i, R_i \mid i = 1 \dots 4\}$. Open circles M_i 's are unknown world points lying on π_k ;
C and C' are the perspective center of the camera and projector.....15

Fig.12 (a) The Calibration box, have six calibration lines and eighteen known world positions.
(b) 32 strip plane patterns..... 16

Fig.13 Pattern projection classified. [11]18

Fig.14 (a) A sequence of binary patterns are projected in order to divide in the object in
regions (b) An additional periodical pattern is projected19

Fig.15 coded structured system.....20

Fig.16 single pattern frame sequences. (table tennis bag).....20

Fig.17 (a) original real image, (b) our scanning result, (c) polygonal result..... 25

Fig.18 Dipole configuration for semi-infinite geometry29

Fig.19 Optimization flow chart..... 33

Fig.20 The proposal System.....34

Fig. 21 Bunny original image (a) frontal view, (b) rear view35

Fig.22 Bunny with position noise (random noise per vertex)36

Fig.23 Synthetic bunny images.....37

Fig.24 Phase 1 Optimization.....38

Fig.25 Round 2 reflectance optimized data.....39

Fig.26 Synthetic bunny image (by BSSRDF model).....40

Fig.27 Result position optimized data.....41

Fig.28 Input structured light images.....42

Fig.29 (a)an input reflectance image (b) scanned data.....43

Fig.30 The left image shows real reflectance color, and the right image shows optimized
reflectance color.....44

Fig.31 The result of Phong optimized position.....45

Chapter 1. Introduction

1.1 Background

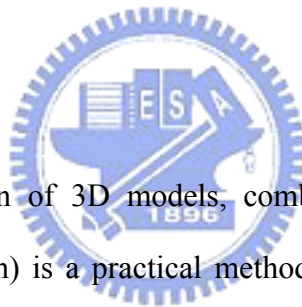
Recently, the requirement of digitizing 3D models and estimating surface parameters from real objects is increased dramatically. They are extensively used in computer graphics, computer vision, and other analysis applications. 3D acquisition can be categorized into several principal approaches: passive stereo, active stereo, shape from shading, photometric stereo, etc. Each of them has its advantages and disadvantages.

Passive stereo methods use multiple images captured from difference viewpoints. Then, they estimate the correspondences between images and calculate 3D positions by intersecting corresponding pairs. The major benefit of passive stereo is easy to implement and it requires only two or more cameras. But, estimating the exact correspondence between images is difficult, and therefore the accuracy of the data may be unreliable.

Active stereo utilizes additional light sources or laser projectors for scanning, and thus the correspondences between two images are easier to be acquired. The accuracy of active stereo approaches is therefore relatively high. On the other hand, the active stereo systems usually require additional projection devices which are usually heavy and costly. However, the surface details of non-lamertian material objects are usually difficult to be acquired by active stereo or passive stereo since correspondences on details are usually ambiguous and the reflection properties are not taken into account.

Shape from shading and photometric stereo methods make use of shading information to recover the 3D shape. Most works on photometric stereo are based on the lambertian model. They usually use a single view direction, but various lighting directions. The normal estimation then become a simple linear least-square problem. But the accuracy may be not reliable because the objects are not always with lambertian reflection properties and reconstructing surface from normal variations is ill-condition. Shape from shading (SFS) uses intensity variation of a single image and known lighting conditions to recovery 3D shape. The problem of finding correspondences can be avoided in shape from shading, but the solution of shape from shading relies on image quality and accurate reflectance models. Shapes recovered by shape from shading are usually tainted due to input noise or simplified reflectance models.

1.2 Motivation



For accurate reconstruction of 3D models, combining both positions and reflectance properties (shading information) is a practical method. Diego (2005) et al. [1] proposed an impressive approach to combine 3D positions and normals for precise 3D geometry. They measured the positions and normals by a structured light system and a photometric stereo method respectively. In order to efficiently combine the positions and normals by linear cross products, they assume the objects are with lambertian properties and only use lambertian reflectance model to acquire normals.

However, non-lambertian and sub-surface scattering materials are commonly found in the natured world. The lambertian reflectance model is insufficient to represent the greater part of objects. A simpler non-lambertian model for shape recovery is purposed by Tianli (2004) et al [2]. They apply the Phong reflectance model to model the surface reflectance and then used visual hull to find the initial shape. Then, an optimization approach, conjugate gradient, is

purposed to find the shape and reflectance parameters that fit multiple views images. Although, the specular reflection is taken into account and visual hull is used for initial positions. The sub-surface scattering material objects are still not easy to be reconstructed by their method. This problem is still a bottleneck of the reconstruction. In general, to scan these objects, operators usually apply powders or paints on the surface to avoid dealing with non-lambertian properties. The painting process is inconvenient and not applicable for valuable objects.

1.3 Purpose

To tackle the above mentioned problems, in this thesis, we present the use of the stereo structured light to acquire the initial positions. And then, Phong model and Bidirectional Scattering Surface Reflectance Distribution Function model (BSSRDF) are used to optimize the positions of scanned 3D geometry and also acquire the reflectance properties. For the BSSRDF model, Jensen et al. (2001) [3] introduced a dipole diffusion approximation for light scattering. This approximation uses an extension to diffusion theory.

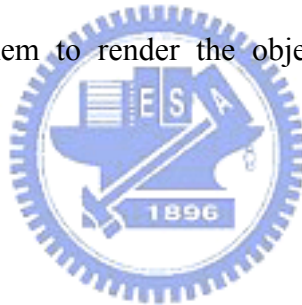
We make use of these models to compensate scanned 3D geometry of the non-lambertian or sub-surface scattering objects. Our method is performed in three steps: First, a projective stereo structured light system is used to acquire the initial positions and normals. Second, assume the light and camera locations are known, we simplify the Phong model and Jensen's model. Then, we use the simplify models to acquire the optimize reflectance parameters. The optimization method we apply is conjugate gradient. It minimizes the difference between synthesized images and the real images. Last, using the estimated reflectance parameters, we can further optimize the position with conjugate gradient. In order to get a more precise shape and reflectance properties, we can repeat the step 2 and step 3. Finally, we can reconstruct a

most accurate 3D model and reflectance properties.

1.4 Contribution

In the thesis, we propose an approach to combine 3D scanned data and reflectance properties for precise 3D surface. The primary research goals and features are addressed as follows:

- (a) Improving the scanning accuracy of non-lambertian and sub-surface scattering objects.
- (b) Utilizing only inexpensive devices.
- (c) The method is not only reconstructing the shape but also estimating the reflectance properties. We can use them to render the object from different views and lighting conditions.



1.5 System Overview

Our goal is to recover a high quality 3D geometry from images. We combined the positions measured by structured light system and Phong or BSSRDF reflectance model to optimize the reconstructed result. We separate our method into three steps, and the system overview is as follows:

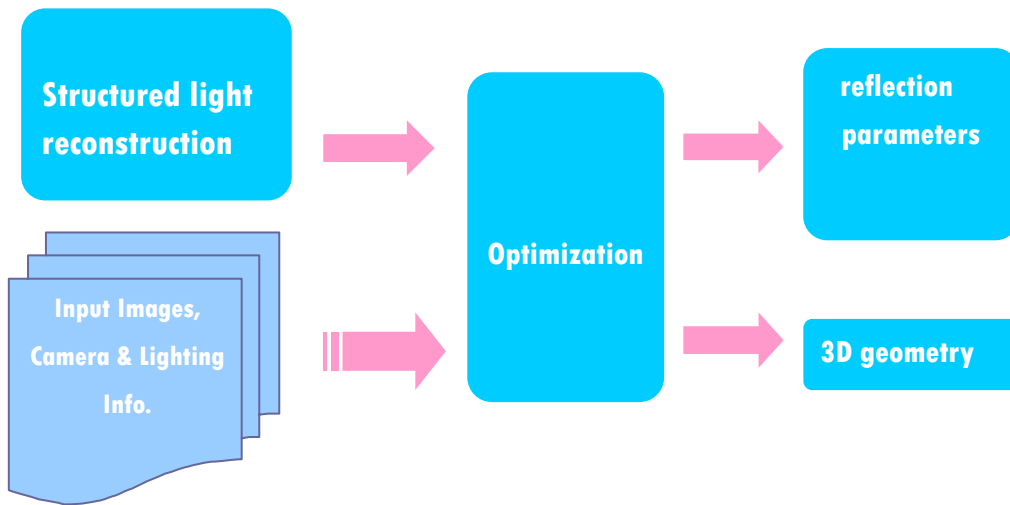


Fig.1 System overview.

1.6 Organization



This thesis is organized as follows. Chapter 2 is about related work, we will review the literature on structured light systems, BSSRDF reflectance model, and combining techniques. Chapter 3, 4 propose our method of surface detail optimization. Various issues such as initialization, reflectance model, and stereo structured light system will also be discussed. Chapter 5 shows the experiment results on real and synthetic objects. Chapter 6 presents the conclusion and future work.

Chapter 2. Related work

In this chapter, we review the literature on 3D recovery, light diffusion reflectance model, and combining techniques. First, we will survey the previous works about 3D recovery techniques and introduce the Du Q.'s et al. [4] calibration method. Then, the difference among BSSRDF reflectance models are described respectively. Finally, we introduce the combining algorithm for precise 3D surface.

2.1 Acquisition of 3D geometry

3D reconstruction can be divided into two basic categories: one is stereo triangulation approach, and another is shape from lighting or shading variations. In these decades, range scanning technologies based on stereo triangulation have become the main stream, since they are flexible, inexpensive, and accurate. Chen and Kak (1987) [5] proved that image coordinates can be directly transformed to the world coordinate via a transformation matrix in active triangulation systems. They incorporated the laser range finder and a robot arm. World lines could be generated by moving the robot arm and the scanner to different known positions. Zhang (2003) et al. [6] extends the traditional binocular stereo problem into the spacetime domain, where a pair of video streams is matched simultaneously instead of matching pairs of images frame by frame. The spacetime stereo framework has proved effective for reconstructing shape from changes in appearance (**Fig.2**).

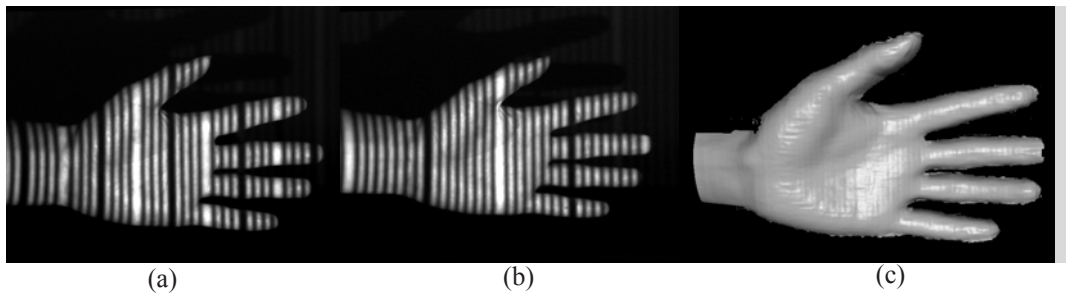


Fig.2 (a), (b) Two images taken from one of the cameras. (c) Shaded rendering of the reconstructed model by window spacetime analysis.[6]

Photometric stereo and shape from shading recover the shape using lighting information. Aaron (2005) et al. [7] presents a technique for computing the geometry of objects with general reflectance properties from images. They assume the camera viewpoint is fixed, but the illumination varies over the input sequence. They put the target object and example objects with the same materials under the same illumination conditions. Since the geometry of the example object are known, they use the orientation-consistency to measure the real object's normals (**Fig.3**).



Fig.3 Reconstruction by examples. (a) Input data (one of 13 sets). (b) Views of the reconstructed model.[7]

Fang (2004) [8] et al. use shape from shading techniques to recover a height field from images and combine them with a texture synthesis method to create a new texture editing tool.

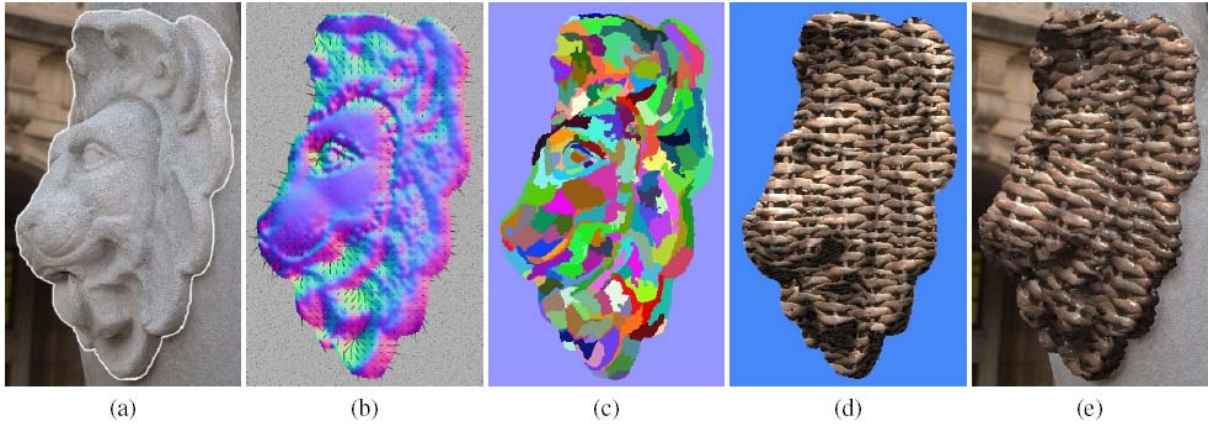


Fig.4 (a) An ordinary photo. (b) Shape-from-shading applied to an object in the image to estimate its normals. (c) Pixel patches formed by clustering normals. (d) Texture synthesized on these patches and aligned with neighboring patches. (e) Final result with texture orientation distortion, displacement mapping and environment mapping.[8]

G. Vogiatzis et al. [13] provide a novel approach, volumetric graph-cuts. Their algorithm proposed uses the visual hull of the scene to infer occlusions and as a constraint on the topology of the scene. A photo consistency-based surface cost function is defined and discretised with a weighted graph. A viewpoint independent surface is reconstruction.(**Fig.5**)



Fig5. Clay horse. Left column: Images of the clay horse sequence. Right column: Similar view-points of the reconstructed model using graph-cuts.[14]

Because our structured light system is modified from a projective calibration method by Du Q. and Huynh (1997) [4], we will briefly their method here. They presented a novel calibration method that based on cross ratio invariant theorem. They used 4 known non-coplanar sets of world point for calibration. The direct 4x3 image-to-world transformation matrix for each light stripe plane can also be recovered from plane-to-plane homography (**Fig.6**).

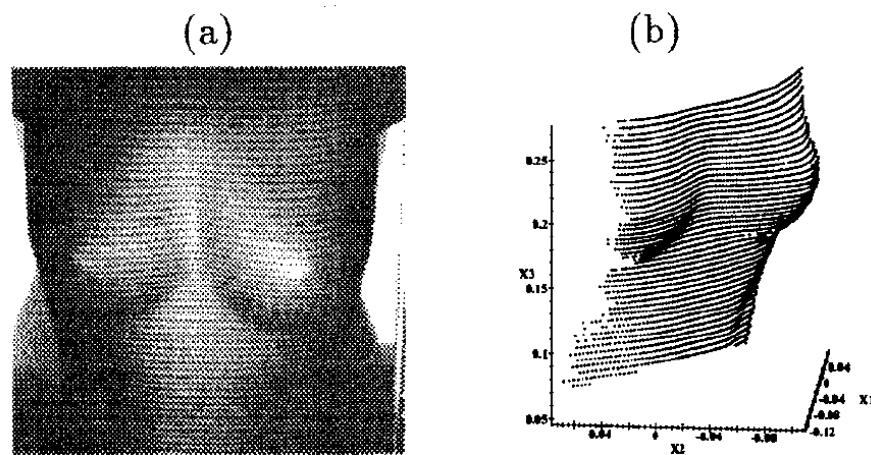


Fig6. (a) input image data. (b) result model.[4]

2.2 Light diffusion reflection model

Most reflectance models are derived from surface scattering, without any subsurface scattering. They assume the light entering a material and leave the material at the same position. However, reflection contributed by sub-surface scattering is ignored by these assumptions.

Therefore, Nicodnmus (1977) et al. [9] proposed the Bidirectional Scattering Surface Reflectance Distribution Function (BSSRDF) to describe a scattering of light in translucent materials.

$$S(x_i, \vec{\omega}_i, x_o, \vec{\omega}_o) = \frac{dL(x_o, \vec{\omega}_o)}{d\Phi(x_i, \vec{\omega}_i)} \quad (1)$$

Here L is outgoing radiance, Φ is incident flux, x_i and $\vec{\omega}_i$ the incidence position and direction, and x_o and $\vec{\omega}_o$ the exiting position and direction. The BSSRDF can describe light transport between any two rays that hit a surface and the translucent materials can be captured. Jensen (2001) et al. [3] introduces a BSSRDF model that combines a dipole diffusion approximation with an single scattering computation. They also showed how the model can be used to measure the scattering properties of translucent materials, and how the measured values can be used to reproduce the results of the measurements as well as synthetic rendering (**Fig.7**).

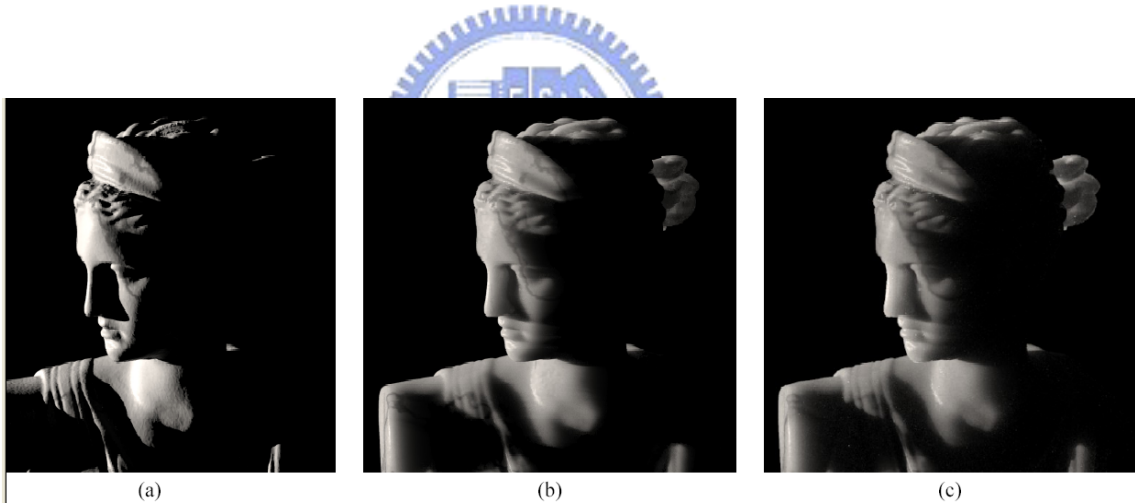


Fig.7 A simulation of subsurface scattering in a marble bust. The marble bust is illuminated from the back and rendered with: (a) the BRDF approximation (b) the BSSRDF approximation, and (c) a full Monte Carlo simulation. [3]

Based on Jensen's approach, Craig (2005) et al. [10] presented a new efficient technique with multiple dipoles to account for diffusion in thin slabs. They also extended this multipole theory to account for both surface roughness and layers with varying indices of refraction, and then they combined it with a novel frequency space application of Kubelka-Munk theory in order to simulate light diffusion in multi-layered translucent materials. Their approach is more

general and can be used for arbitrary numbers of layers, and it enables the composition of arbitrary multi-layered materials with different optical parameters at each layer (**Fig.8**).



Fig.8 A multi-layered model of human skin using measured parameters for the individual skin layers[10]

2.3 Combining algorithms

In order to obtain high-quality 3D geometry, combining positions and shading information can be a considerable solution. Diego (2005) et al. [1] purposed a two-phase hybrid reconstruction algorithm for precise 3D geometry. In the first phase, they used positions to improve normals. Let N^m and N^p be the normal field indirectly obtained from measured positions and the directly measured normal field respectively. They planed to replace the low-frequency component of N^m with data from N^p . They used a structured light system for original positions, and they used photometric stereo method for directly measured normals. The second phase was using measured normals to improve positions. They minimized the errors by a linear least square method. It is an efficient approach but they can only deal with

lambertian objects (**Fig.9**).



Fig.9 least square optimization. (Left) Several range scans were aligned and merged. (Right) The result was later optimized with mapped normals coming from several independent photometric stereo scans.[1]

Tianli (2004) et al. [2] presented an algorithm to simultaneously estimate both the 3D shape and parameters of a surface reflectance model from multiple views of an object with a single material. First, the rough initial shape is acquired by visual hull. Then, they chose the Phong reflectance model as the parametric reflectance model and they used the initial shape to minimize the cost function to find the better reflectance properties. The cost function is the sum of the difference between synthesis images and real images. Finally, they fixed reflectance properties and refined 3D shape similar to above-mentioned steps. The whole process continues until the cost function no longer decreases or progress of decrease is small. They also handle self-occlusion and self-shadowing problem by checking the triangle's visibility based on the current estimate of the shape at each steps of the minimization process. However, in their experiments they only apply their work on synthetic images and a real object with near-spherical surface (**Fig.10**).

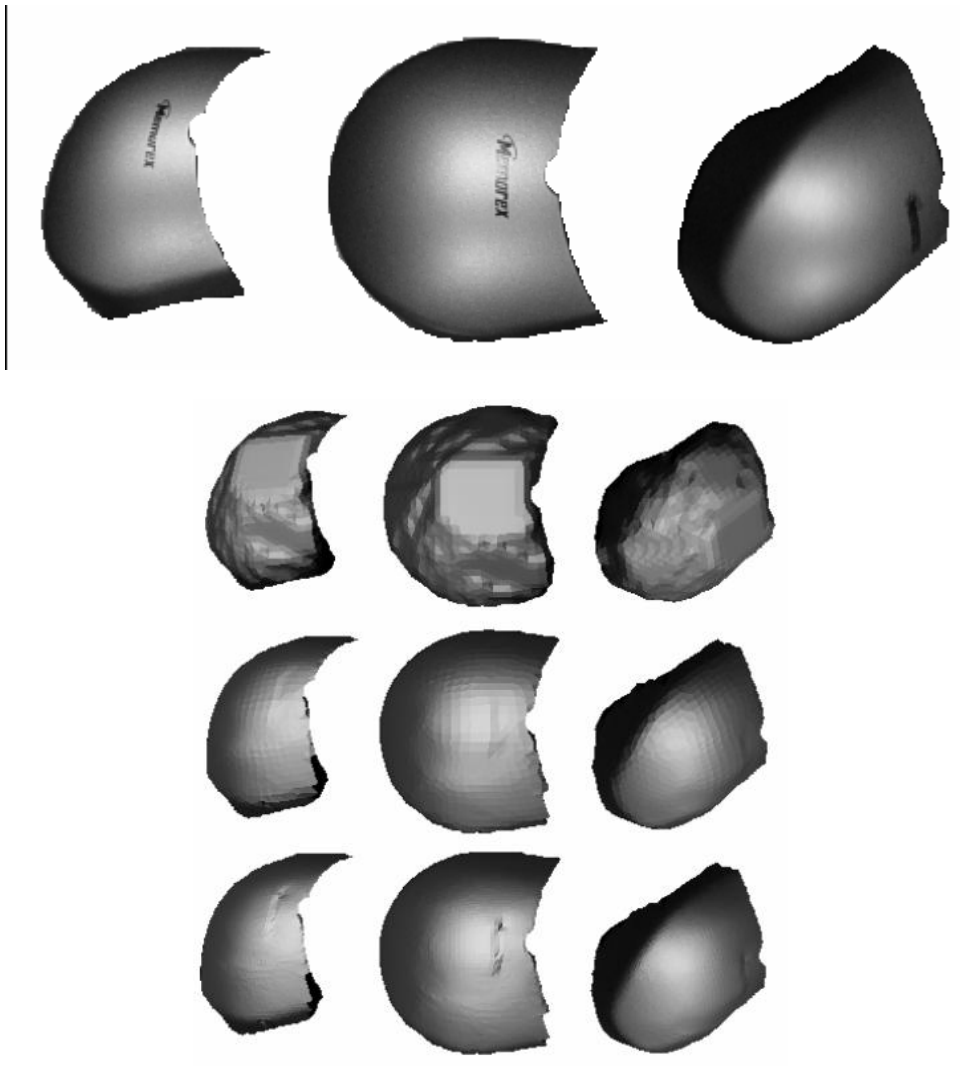


Fig. 10 1nd row input images of a real mouse, down: 2nd row. Optimized reflectance model with the initial shape. 3rd row. Optimized results at the 1st step. Optimized results at 2st step.[2]

Chapter 3. Acquisition of positions

In this chapter, we use a projective calibration method proposed by Du Q. and Huynh 1997 [4] to construct a structured light system. Our structured light system can be performed in three phases: (1) projector calibration, (2) coded structured light, (3) image-to-world transform.

3.1 Projector calibration

The goal of our projector calibration stage is to estimate the plane equation of each light stripe. The unknown coefficients a , b , c , and d represent a plane:

$$aX_1 + bX_2 + cX_3 + d = 0. \quad (2)$$

In order to find the coefficients in (2), at least 3 non-collinear world points that fall onto the stripe plane must be known. It is difficult to recover all of them onto all of stripe planes. Therefore we make use of cross ratio properties. As showing in Fig 7, given 4 non-coplanar sets $\{P_1, Q_1, R_1\}$ $\{P_2, Q_2, R_2\}$ $\{P_3, Q_3, R_3\}$ $\{P_3, Q_3, R_3\}$, we can use the cross-ratio properties to estimate the intersection M_1, M_2, M_3, M_4 . The 4 points will then be used to evaluate the plane equations (**Fig.11**).

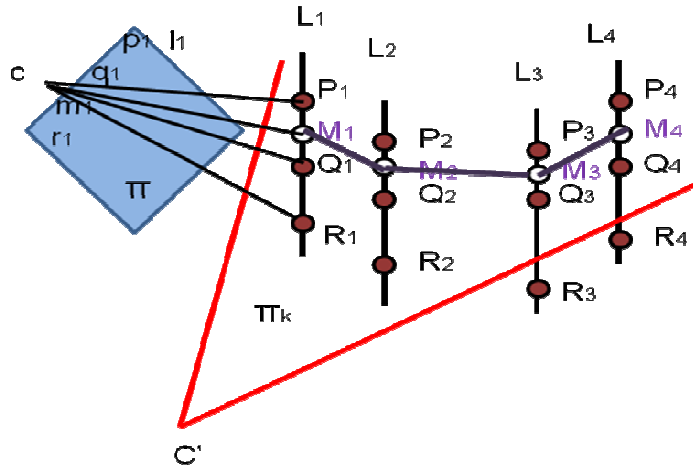


Fig.11 Projective calibration using 3 known non-coplanar sets of 3 collinear world points (dark circles $\{P_i, Q_i, R_i \mid i = 1 \dots 4\}$). Open circles M_i 's are unknown world points lying on π_k ; C and C' are the perspective center of the camera and projector.

3.1.1 Cross ratio

Give 4 collinear points p, q, r, m lying on a line l, we can express points on l in the following form:



$$(q - p)\theta + p, \tag{3}$$

where θ is the parameter that defines points on the line. This parameterization gives $\theta_p = 0$, $\theta_q = 1$, θ_r and θ_m any real numbers depending on their positions relative to p on the line. The cross ratio $\{p, q; r, m\}$ of these points are defined as:

$$\{p, q; r, m\} = \left(\frac{\theta_p - \theta_r}{\theta_q - \theta_r} \right) / \left(\frac{\theta_p - \theta_m}{\theta_q - \theta_m} \right) \tag{4}$$

Since the cross ratio is invariant under perspective projection if 4 world points P, Q, R, M are

collinear, then their image projections p, q, r, m are also collinear and the same cross ratio.

3.1.2 Calibration box

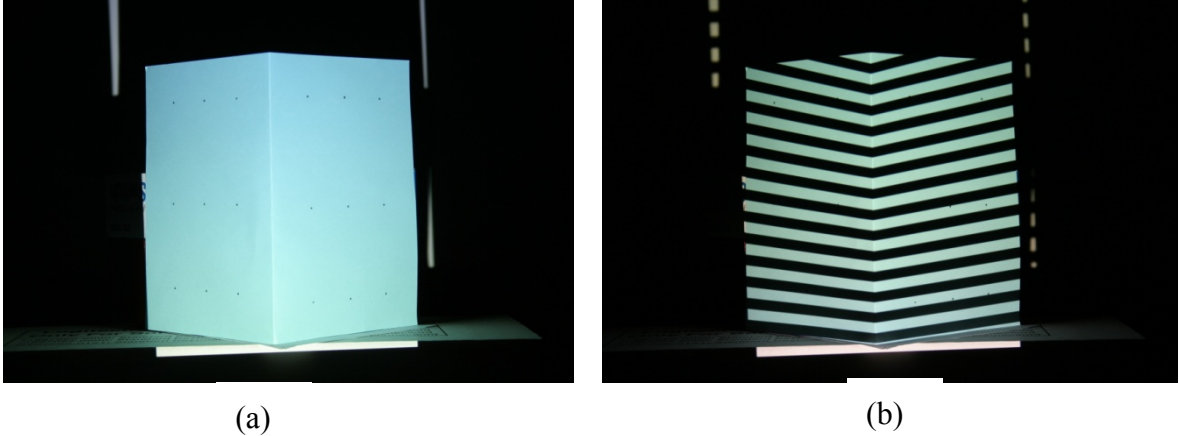


Fig.12 (a) The Calibration box, have six calibration lines and eighteen known world positions. (b) 32 strip plane patterns.

In order to obtain the accurate stripe plane equations and a camera model, we use a calibration box (**Fig.12**). When we fix the camera and projector, the camera model and stripe plane equations will not change. We can obtain world positions easily and a more accurate data.

3.1.3 Computing the stripe plane

Since the 4 world points $M_i, i = 1 \dots 4$ lying on the stripe plane have been determined, we use these four world points to find the coefficients on equation (2).

Equations:

$$a_1 X_i + a_2 Y_i + a_3 Z_i + a_4 = 0, i = 1 \dots 4 \quad (3)$$

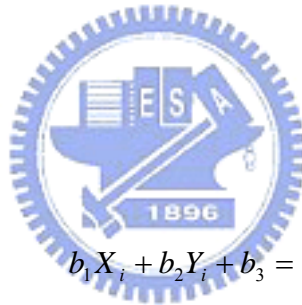
We solve them by the pseudo-inverse method. Unfortunately, this equation has a degenerate solution when all the coefficients are zero. To avoid the situation, we can reformulate them by dividing across by a_3 and letting:

$$\begin{aligned} \frac{a_1}{a_3} &= b_1 \\ \frac{a_2}{a_3} &= b_2 \\ \frac{a_4}{a_3} &= b_3 \end{aligned} \quad (4)$$

Thus:

$$b_1 X_i + b_2 Y_i + Z_i + b_3 = 0 \quad (5)$$

, and hence:



$$b_1 X_i + b_2 Y_i + b_3 = -Z_i \quad (6)$$

A least-square-error solution to this set of equations can be written in matrix form as:

$$\begin{bmatrix} X_1 & Y_1 & 1 \\ X_2 & Y_2 & 1 \\ X_3 & Y_3 & 1 \\ X_4 & Y_4 & 1 \end{bmatrix} * \begin{bmatrix} b_1 \\ b_2 \\ b_3 \end{bmatrix} = \begin{bmatrix} -Z_1 \\ -Z_2 \\ -Z_3 \\ -Z_4 \end{bmatrix} \quad (7)$$

By using the pseudo-inverse method, the equation of the stripe is then found.

3.1.4 Adjust the normal on stripe plane

Because not all of the 4 world points $M_i, i=1 \dots 4$ lying on the stripe plane can be found, the estimated plane normal may not be reliable. We use all of the stripe plane's normals, perspective projection, and collinear property to adjust each other and then the more accurate normals can be evaluated.

3.2 Coded structured light

THE PROPOSED CLASSIFICATION



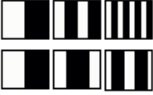

		Maruyama and Abe	Durdle et al.	Ito and Ishii	Boyer and Kak	Chen et al.
Spatial neighborhood	Non-formal codification	✓	✓	✓	✓	✓
	De Bruijn sequences 	✓	✓	✓	✓	✓
	M-arrays 	✓	✓	✓	✓	✓
Time-multiplexing	Binary codes 	✓	✓	✓	✓	✓
	n-ary codes	✓	✓	✓	✓	✓
	Gray code + Phase shifting	✓	✓	✓	✓	✓
	Hybrid methods	✓	✓	✓	✓	✓
Direct coding	Grey levels	✓	✓	✓	✓	✓
	Colour 	✓	✓	✓	✓	✓
Scene applicability		Static				
Pixel depth		Binary				
Coding strategy		Periodical				
		Absolute				

Fig.13 Pattern projection classified. [11]

3.2.1 Binary coded and phase shifting

In order to find the correspondence easier, we use a coded structured light approach. Coded structured light system consists of cameras and a projector that projects light patterns onto the surface. **Fig.13** shows the survey of pattern projection techniques, and they are classified according to their codification strategy. We encoded each point in binary codes (**Fig.14a**) and shift phases (**Fig.14b**) that will help us identify its coordinates. These binary codes are easy to implement and we use the additional shift images to reduce the coded length and coded errors.

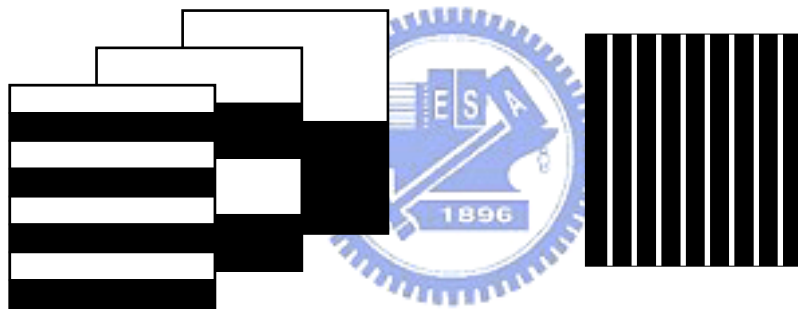


Fig.14

(a) A sequence of binary patterns are projected in order to divide in the object in regions

(b) An additional periodical pattern is projected

In this experiment, we constructed a test bed (as shown in **Fig.15**) that consists of a camera and a projector. We encode the white stripe as 1 and the black one as 0. With careful design of codes, the projection coordinated can be estimated much easier.

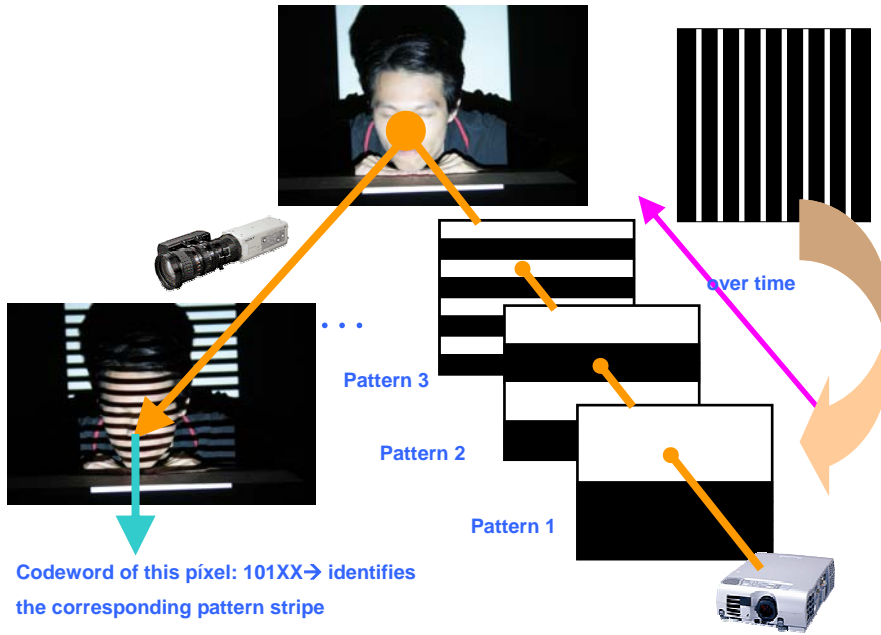


Fig.15 coded structured system

3.2.2 Single-stripe sequence

For obtaining more accuracy data, we can also use the traditional single pattern to define the stripe plane.

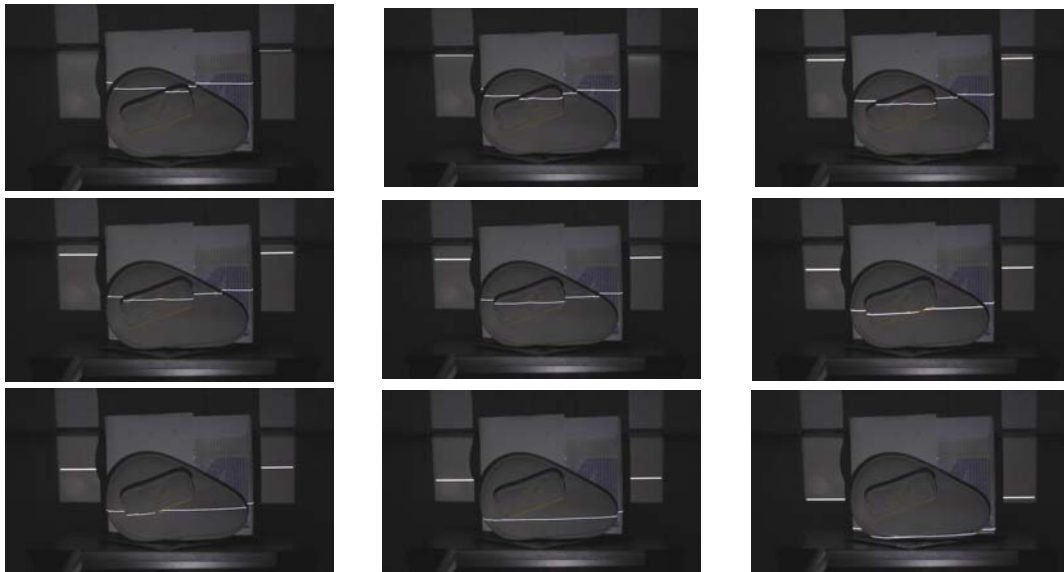


Fig.16 single pattern frame sequences. (table tennis bag)

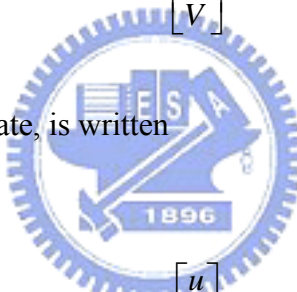
3.3 Computing the image-to-world transformation

After projective calibration and finding correspondence, we can recover the 3D position from 2D image. First we make use of 12 known feature points to estimate the camera parameters and then the image-to-world transformation matrix will be defined.

3.3.1 Estimate camera model

Let the points in the image coordinate

which in homogeneous coordinate, is written


$$\begin{bmatrix} U \\ V \end{bmatrix}$$
$$\begin{bmatrix} u \\ v \\ t \end{bmatrix}$$

Thus:

$$U = \frac{u}{t} \quad (8)$$

, and:

$$V = \frac{v}{t} \quad (9)$$

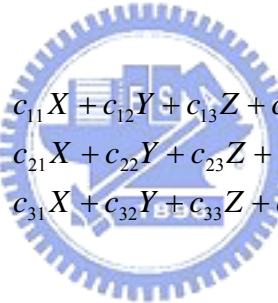
Let the desired camera model, a transformation which mapping the three-dimensional world point to the corresponding two-dimensional image point, be C. Thus:

$$C \begin{bmatrix} x \\ y \\ z \\ 1 \end{bmatrix} = \begin{bmatrix} u \\ v \\ t \end{bmatrix} \quad (10)$$

Hence C must be a 3 x 4 homogeneous transformation:

$$C = \begin{bmatrix} c_{11} & c_{12} & c_{13} & c_{14} \\ c_{21} & c_{22} & c_{23} & c_{24} \\ c_{31} & c_{32} & c_{33} & c_{34} \end{bmatrix} \quad (11)$$

Expanding this matrix equation, we get:



$$\begin{aligned} c_{11}X + c_{12}Y + c_{13}Z + c_{14} &= u \\ c_{21}X + c_{22}Y + c_{23}Z + c_{24} &= v \\ c_{31}X + c_{32}Y + c_{33}Z + c_{34} &= t \end{aligned} \quad (12)$$

and:

$$\begin{aligned} u &= Ut \Rightarrow u - Ut = 0 \\ v &= Vt \Rightarrow v - Vt = 0 \end{aligned} \quad (13)$$

so:

$$\begin{aligned} c_{11}X + c_{12}Y + c_{13}Z + c_{14} - Uc_{31}X - Uc_{32}Y - Uc_{33}Z - Uc_{34} &= 0 \\ c_{21}X + c_{22}Y + c_{23}Z + c_{24} - Vc_{31}X - Vc_{32}Y - Vc_{33}Z - Vc_{34} &= 0 \end{aligned} \quad (14)$$

Because the overall scaling of C is irrelevant due to the homogeneous system and, thus, without the value of c_{34} can be set arbitrarily to 1 and we can rewrite (14) as follows:

$$\begin{aligned}
c_{11}X + c_{12}Y + c_{13}Z + c_{14} + c_{21}0 + c_{22}0 + c_{23}0 + c_{24}0 - Uc_{31}X - Uc_{32}Y - Uc_{33}Z &= U \\
c_{11}0 + c_{12}0 + c_{13}0 + c_{14}0 + c_{21}X + c_{22}Y + c_{23}Z + c_{24} - Uc_{31}X - Uc_{32}Y - Uc_{33}Z &= V
\end{aligned} \quad (15)$$

This reduces the number of unknowns to eleven. For six observations, we now have twelve equations and eleven unknowns. Reformulating the twelve equations in matrix form, we can obtain a least-square-error solution to the system using the pseudo-inverse method.

Let:

$$X = \begin{bmatrix}
x^1 & y^1 & z^1 & 1 & 0 & 0 & 0 & 0 & -U^1x^1 & -U^1y^1 & -U^1z^1 \\
0 & 0 & 0 & 0 & x^1 & y^1 & z^1 & 1 & -V^1x^1 & -V^1y^1 & -V^1z^1 \\
x^2 & y^2 & z^2 & 1 & 0 & 0 & 0 & 0 & -U^2x^2 & -U^2y^2 & -U^2z^2 \\
0 & 0 & 0 & 0 & x^2 & y^2 & z^2 & 1 & -V^2x^2 & -V^2y^2 & -V^2z^2 \\
x^3 & y^3 & z^3 & 1 & 0 & 0 & 0 & 0 & -U^3x^3 & -U^3y^3 & -U^3z^3 \\
0 & 0 & 0 & 0 & x^3 & y^3 & z^3 & 1 & -V^3x^3 & -V^3y^3 & -V^3z^3 \\
x^4 & y^4 & z^4 & 1 & 0 & 0 & 0 & 0 & -U^4x^4 & -U^4y^4 & -U^4z^4 \\
0 & 0 & 0 & 0 & x^4 & y^4 & z^4 & 1 & -V^4x^4 & -V^4y^4 & -V^4z^4 \\
x^5 & y^5 & z^5 & 1 & 0 & 0 & 0 & 0 & -U^5x^5 & -U^5y^5 & -U^5z^5 \\
0 & 0 & 0 & 0 & x^5 & y^5 & z^5 & 1 & -V^5x^5 & -V^5y^5 & -V^5z^5 \\
x^6 & y^6 & z^6 & 1 & 0 & 0 & 0 & 0 & -U^6x^6 & -U^6y^6 & -U^6z^6 \\
0 & 0 & 0 & 0 & x^6 & y^6 & z^6 & 1 & -V^6x^6 & -V^6y^6 & -V^6z^6
\end{bmatrix}$$

$$C = \begin{bmatrix} c_{11} \\ c_{12} \\ c_{13} \\ c_{14} \\ c_{21} \\ c_{22} \\ c_{23} \\ c_{24} \\ c_{31} \\ c_{32} \\ c_{33} \end{bmatrix} \quad y = \begin{bmatrix} U^1 \\ V^1 \\ U^2 \\ V^2 \\ U^3 \\ V^3 \\ U^4 \\ V^4 \\ U^5 \\ V^5 \\ U^6 \\ V^6 \end{bmatrix} \quad (16)$$

$$C = (X^T X)^{-1} X^T y$$

3.3.2 Estimate 3D positions

Once the camera model C has been determined, we can estimate a 3D position in the world coordinate from its projected image position. Recalling equations (12) and (13):

$$\begin{aligned} c_{11}X + c_{12}Y + c_{13}Z + c_{14} &= u = Ut \\ c_{21}X + c_{22}Y + c_{23}Z + c_{24} &= v = Vt \\ c_{31}X + c_{32}Y + c_{33}Z + c_{34} &= t \end{aligned} \quad (17)$$

Substituting the expression for t into the first two equations gives:

$$\begin{aligned} U(c_{31}X + c_{32}Y + c_{33}Z + c_{34}) &= c_{11}X + c_{12}Y + c_{13}Z + c_{14} \\ V(c_{31}X + c_{32}Y + c_{33}Z + c_{34}) &= c_{21}X + c_{22}Y + c_{23}Z + c_{24} \end{aligned} \quad (18)$$

Hence:

$$\begin{aligned} (c_{11} - Uc_{31})X + (c_{12} - Uc_{32})Y + (c_{13} - Uc_{33})Z + (c_{14} - Uc_{34}) &= 0 \\ (c_{21} - Vc_{31})X + (c_{22} - Vc_{32})Y + (c_{23} - Vc_{33})Z + (c_{24} - Vc_{34}) &= 0 \end{aligned} \quad (19)$$

We have:

$$\begin{aligned} a_1X + a_2Y + a_3Z &= -a_4 \\ c_1X + c_2Y + c_3Z &= -c_4 \end{aligned} \quad (20)$$

Where

$$\begin{aligned} a_1 &= c_{11} - Uc_{31} & c_1 &= c_{11} - Vc_{31} \\ a_2 &= c_{12} - Uc_{32} & c_2 &= c_{12} - Vc_{32} \\ a_3 &= c_{13} - Uc_{33} & c_3 &= c_{13} - Vc_{33} \\ a_4 &= c_{14} - Uc_{34} & c_4 &= c_{14} - Vc_{34} \end{aligned} \quad (21)$$

, and the stripe plane equation:

$$b_1X + b_2Y + Z = -b_3 \quad (22)$$

We can obtain a least-square-error solution to the system using the pseudo-inverse method.

$$A = \begin{bmatrix} a_1 & a_2 & a_3 \\ c_1 & c_2 & c_3 \\ b_1 & b_2 & b_3 \end{bmatrix}$$

$$x = \begin{bmatrix} X \\ Y \\ Z \end{bmatrix} \quad b = \begin{bmatrix} -a_4 \\ -c_4 \\ -b_3 \end{bmatrix} \quad (23)$$

$$x = (A^T A)^{-1} A^T b$$

This is the image-to-world transformation formation that maps any given image point lying on the k-th light stripe directly to projective coordinates in world coordinates.

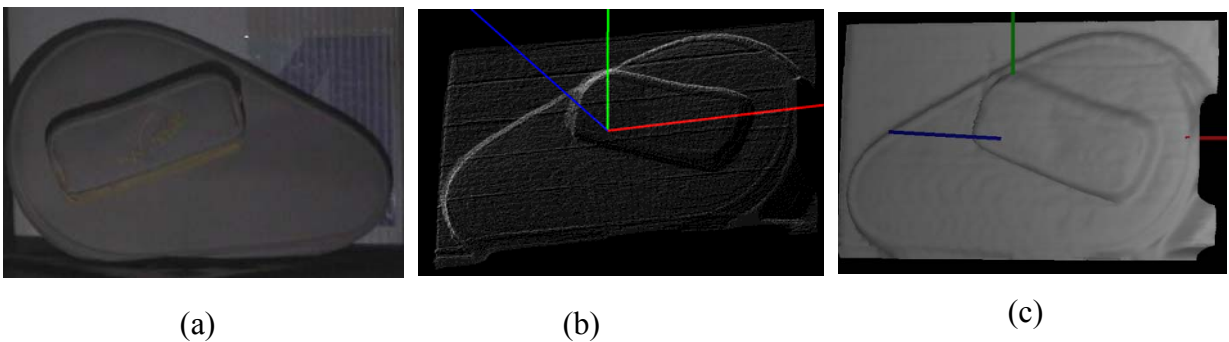


Fig.17 (a) original real image, (b) our scanning result, (c) polygonal result

Chapter 4. Reconstruction and Optimization

After acquiring the stereo positions, we utilize the shape from shading algorithm to optimize the shape surface according to shaded surface intensity. We represent the object surface in terms of a point set. If $\pi : R^3 \rightarrow R^2$ denotes the projection transform from 3D world coordinate to image plane, then the projected point of P_i on the synthesized image in terms of Phong or BSSRDF is:

$$T^i = \langle p_x^i, p_y^i, R^i(Kd, Ks, \alpha, e_i, L) \rangle \quad (24)$$

$$T^i = \langle p_x^i, p_y^i, R^i(\sigma_a, \sigma_s, \eta, e_i, L) \rangle \quad (25)$$

where $p^i = \pi(P^i)$, P (world position), p (image point), and R^i denotes the reflectance value of the point in the synthesized image, computed according to the:

Phong reflectance parameters:

- Kd is the diffuse coefficient
- Ks is the specular coefficient
- α is the shininess coefficient

BSSRDF reflectance parameters:

- σ_s is the scattering coefficient.
- σ_a is the absorption coefficient.
- η is the relative index of refraction.

Joint parameters:

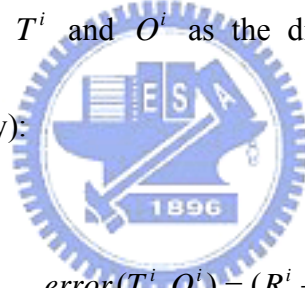
- L is the light source that can illuminate the point p^i
- e_i is the viewing direction.

The observed point corresponding to P_i in the image O^i can be expressed as:

$$O^i = \langle p_x^i, p_y^i, I^i \rangle \quad (26)$$

,where I^i is the intensity value of P_i on input image.

We define the error between T^i and O^i as the difference of R^i (Synthesis reflectance value) and I^i (image intensity):



$$error(T^i, O^i) = (R^i - I^i) \quad (27)$$

When optimizing the positions, we also define a smooth term to restrict the change of the variable between P_i and his neighborhood P_j :

$$smooth(i, j) = (P_x^i - P_x^j)^2 + (P_y^i - P_y^j)^2 + (P_z^i - P_z^j)^2 \quad (28)$$

Finally, we define a cost function C to represent the difference between synthetic and observed images and also the smooth term to represent the reasonableness of estimated surface. Last, the cost function is formed by sum of the squared error and sum of the smooth term between all of the neighborhoods in over all visible points.

When reconstructing the reflectance properties, we define C as follow:

$$C = \sum_{i=1}^n (\text{error}(T^i, O^i))^2 + \sum_{j=1}^m \text{smooth}(i, j) \quad (29)$$

where N is visible point number, and m is neighborhood number.

Through minimizing the cost function, we can evaluate the most appropriate surface and reflectance parameters.

4.1 Reflectance model

Our goal is to reconstruct non-lambertian and sub-surface scattering materials objects. We choose the Phong model for bi-directional reflectance distribution function (BRDF) and a diffusion scattering model for bidirectional scattering surface reflectance distribution function (BSSRDF) as the parametric reflectance model [3].

4.1.1 Phong model

A BRDF can be written as:

$$BRDF = f(\theta_{in}, \phi_{in}, \theta_{ref}, \phi_{ref}) = f(L, V) \quad (30)$$

In this thesis, we apply a commonly-used BRDF model, Phong model (Phong 1975), to optimization the specular reflectance. The equation is written as:

$$R = kd * N \cdot L + ks * (R \cdot V)^\alpha \quad (31)$$

4.1.2 BSSRDF model

In general, the BSSRDF can be approximated by diffusion theory, which accounts for most of the scattered light in natural materials.

$$S_d(x_i, \vec{\omega}_i, x_o, \vec{\omega}_o) = \frac{1}{\pi} F_t(x_i, \vec{\omega}_i) P_d(\|x_i - x_o\|_2) F_t(x_o, \vec{\omega}_o) \quad (32)$$

where F_t is the Fresnel transmittance at the entry and exit points x_i and x_o , and the diffuse reflectance profile, P_d , is approximated by a diffusion dipole.

The dipole approximation was derived for the case of a semi-infinite medium. It assumes that any light entering the material will either be absorbed or return to the surface. Therefore we assume thin slabs break down as light is transmitted through the slab and reduces the amount of light diffusing back to the surface (Fig.18).

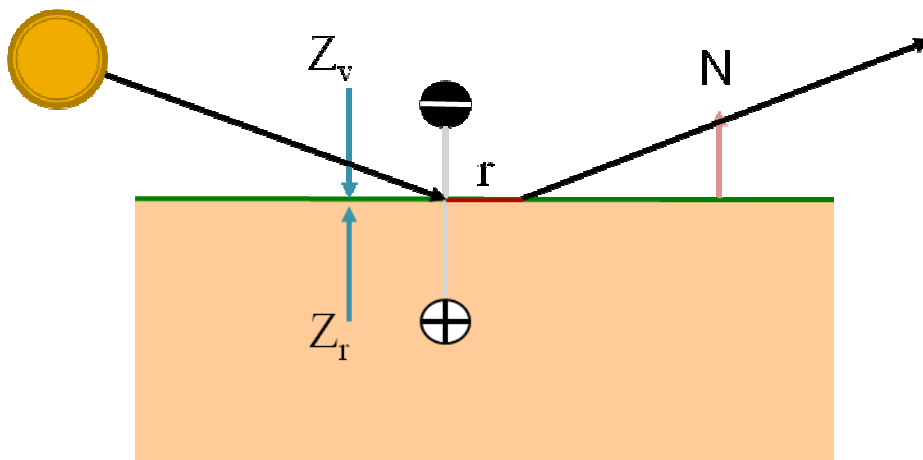


Fig.18 Dipole configuration for semi-infinite geometry.

The reflectance is simply the sum of their individual contributions

$$R(r) = \frac{\alpha' z_r (1 + \sigma_{tr} d_{r,i}) e^{-\sigma_{tr} d_r}}{4\pi d_r^3} - \frac{\alpha' z_v (1 + \sigma_{tr} d_{v,i}) e^{-\sigma_{tr} d_v}}{4\pi d_v^3} \quad (33)$$

where $\sigma_{tr} = \sqrt{3\sigma_a\sigma'_t}$ is the effective transport coefficient, $\sigma'_t = \sigma_a + \sigma'_s$ is the reduced extinction coefficient, $\alpha' = \sigma'_s / \sigma'_t$ is the reduced albedo, σ_a and σ'_s are the absorption and reduced scattering coefficients, and $r = \|x_o - x_i\|$, $d_r = \sqrt{r^2 + z_r^2}$, $d_v = \sqrt{r^2 + z_v^2}$ are the dipole sources from a given point on the surface of the object. The positive real light source, is located at the distance $Z_r = 1/\sigma'_t$, and the other, the negative virtual light source, is located

above the surface at a distance $Z_v = Z_r + 4AD$ where $D = \frac{1}{3\sigma'_t}$ is the diffusion constant and A is defined as:

$$A = (1 + F_{dr}) / (1 - F_{dr}) \quad (34)$$

, and it represents the change in fluence due to internal reflection at the surface. The diffuse Fresnel reflectance F_{dr} can be approximated by the following polynomial expansions (Egan et al. 1973).

$$F_{dr} \cong \begin{cases} -0.4399 + \frac{0.7099}{\eta} - \frac{0.3319}{\eta^2} + \frac{0.0636}{\eta^3}, \eta < 1 \\ -\frac{1.4399}{\eta^2} + \frac{0.7099}{\eta} + 0.6681 + 0.0636\eta, \eta > 1 \end{cases} \quad (35)$$

,where η is the ratio of indices refraction.

4.2 Optimization

In order to acquire a more accurate results, we use the three- layers approach for reliable optimization. First, we only use lambertian diffuse reflectance to optimize the greater part of the normals and the positions. Second, the Phong reflectance model is used to recover the specular part. Last, the sub-surface scattering parameters are obtained and the partial detail of the surface is optimized by BSSRDF.

Our cost function (Equation 29.) has two set of parameters, reflectance parameters and position parameters. We assume a single set of reflectance parameters for all facets, and the positions affect only local. The initial parameters need to avoid poor-conditioning and reflectance-dominance situation, we separated it into two stages in every layers (**Fig.19**): First, we use structured light positions to improve reflectance parameters. And then, we use above reflectance parameters to improve positions.



4.2.1 Using positions to improve reflectance

We start with structured light positions of the object and minimize the cost function (Eq. 32) to find a better set of reflectance parameters. In each phase, first, we fix positions and approximate R until the cost function no longer decrease or the progress of decrease is small. We treat the minimization of cost function as a non-linear problem and obtain a solution by Broydon-Fletcher-Goldfarb-Shanno (BFGS) method. It is a quasi-Newton method and is one of the most popular of variable metric methods. The former converges to the inverse of the Hessian, while the latter converges to the Hessian itself. If we take the derivative of cost function with respect to R parameters, we get:

$$\begin{aligned} \frac{\delta C}{\delta R} &= \frac{\sum_{i=1}^n error(T^i, O^i)^2}{\delta R} \\ &= 2 \sum_{i=1}^n error(T^i, O^i) * \frac{\delta error(T^i, O^i)}{\delta R} \end{aligned} \quad (36)$$

4.2.2 Using reflectance to optimize the positions

After finding a better set of reflectance parameters, we fix R, and refine positions. It is similar to the above steps and we can continue the process until the cost function variation is small or then a threshold.



4.2.3 Optimization Flow Chart

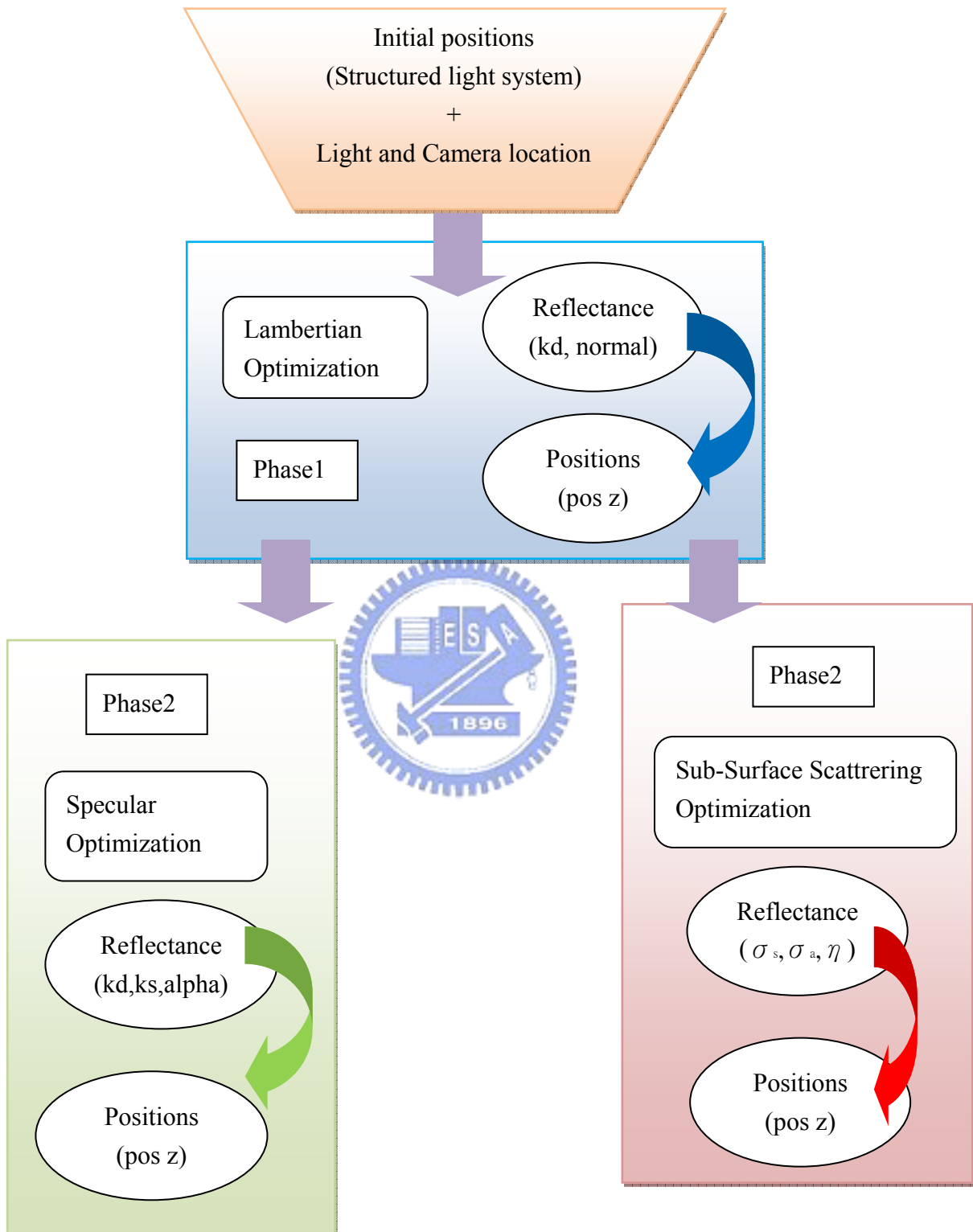


Fig.19 Optimization flow chart

Chapter 5. Experiment and Result

In this chapter, we describe our experiment and results. There are two kinds of experiments. The first one is a synthesis experiment. We use a bunny from Stanford PLY file. We rendered the bunny with reflectance model and add noise to z values of each point as initial position guesses. Then, we perform our algorithm to evaluate the benefit of shading information. Second, we scanned a real data, a marble statue, and optimized it with our algorithm. The framework is implemented in C++, OpenGL and WIN 32 library with a Pentium4 3.20GHz CPU and 1.5 G RAM. The proposed system is show in Fig 20:

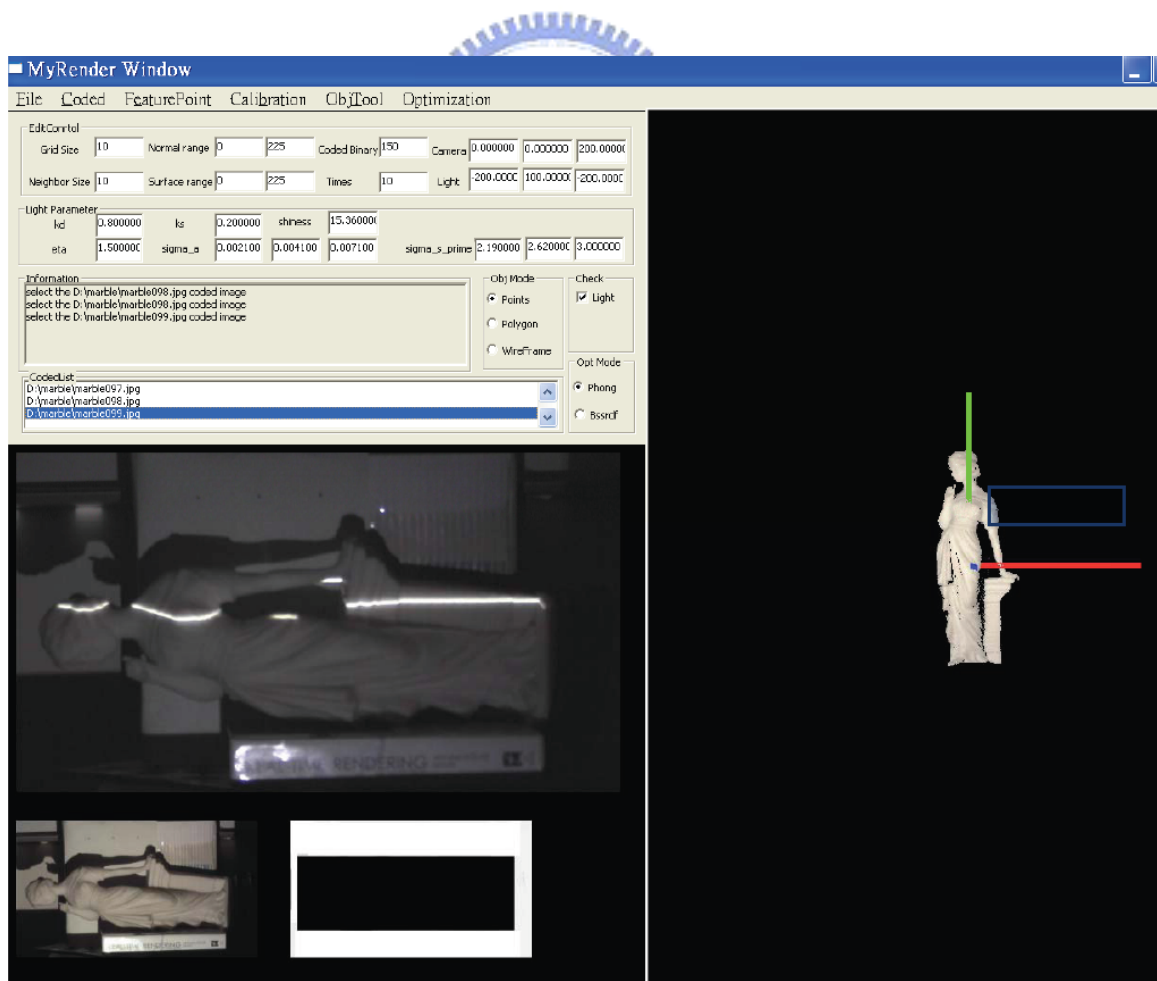


Fig.20 The proposal System

5.1 A Bunny

Table1.

data information	
Vertex number	35,947
Polygon number	69,451

Original data

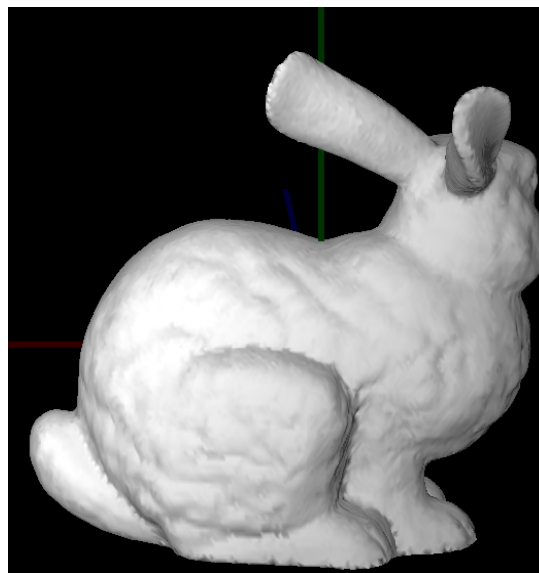
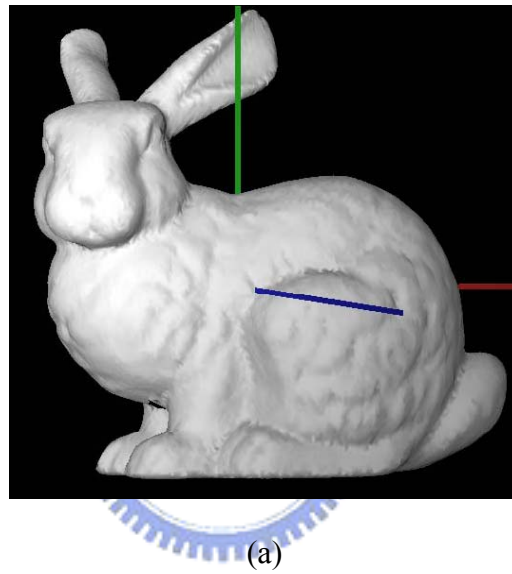
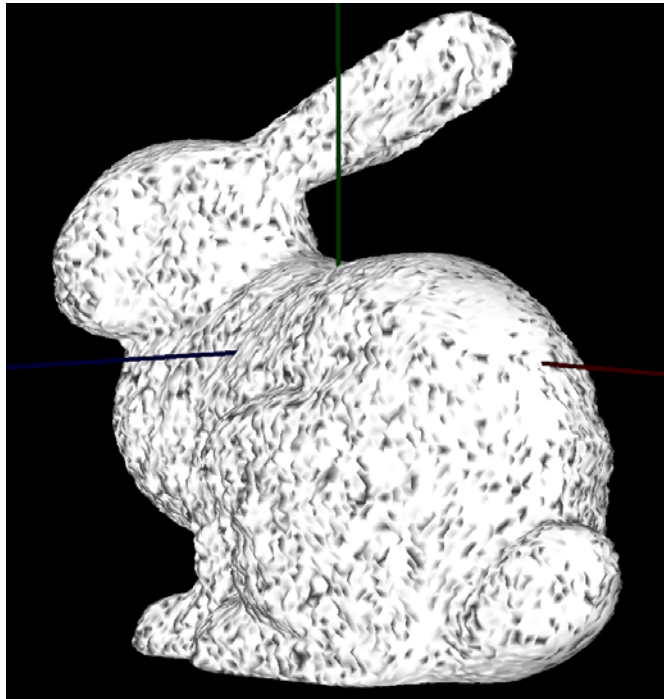
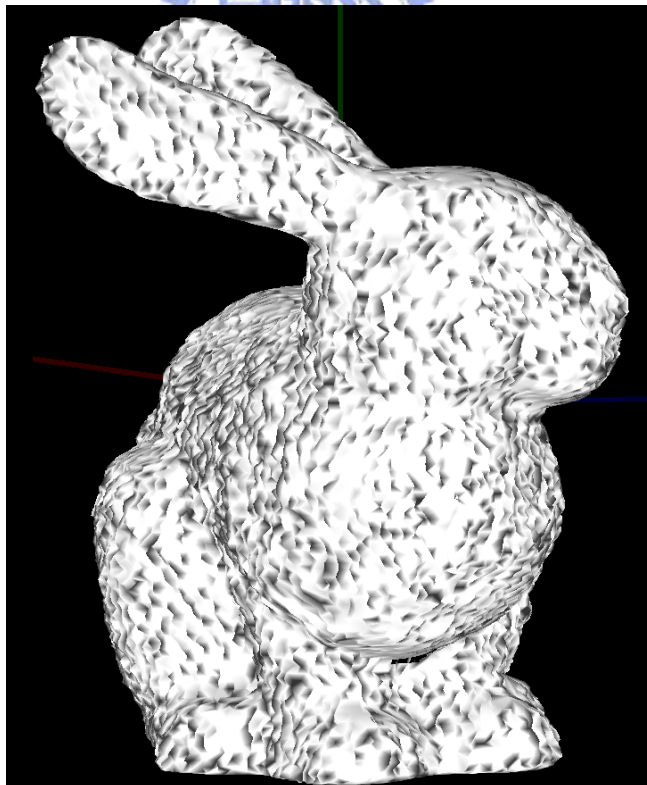


Fig. 21 Bunny original image (a) frontal view, (b) rear view

Noise Model



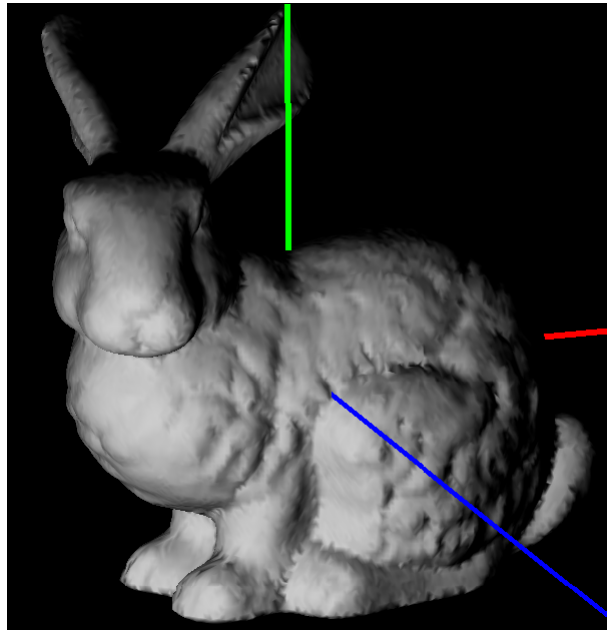
(a)



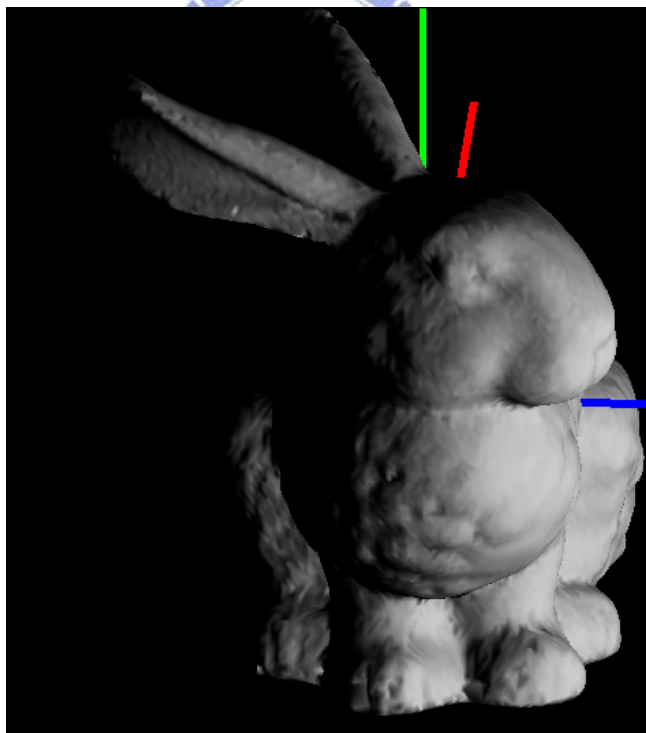
(b)

Fig.22 Bunny with position noise (random noise per vertex)

Synthesis Reflectance



(a)



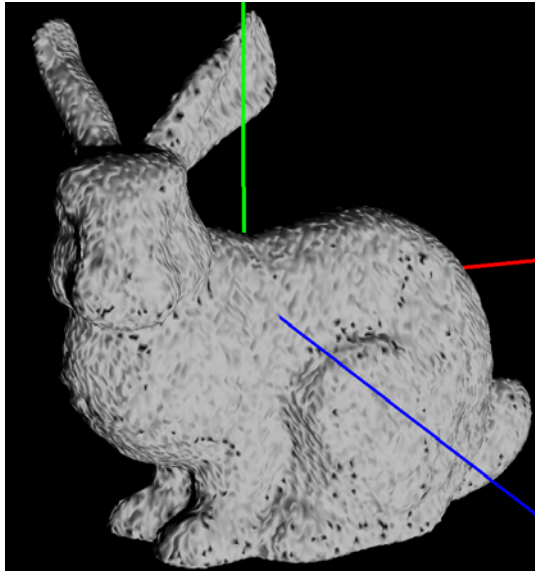
Phong Model: $k_d=0.8, k_s=0.2, \alpha=0.5$ Camera(0,0,1000) Light(0,0,1000)

(b)

Fig.23 Synthetic bunny images

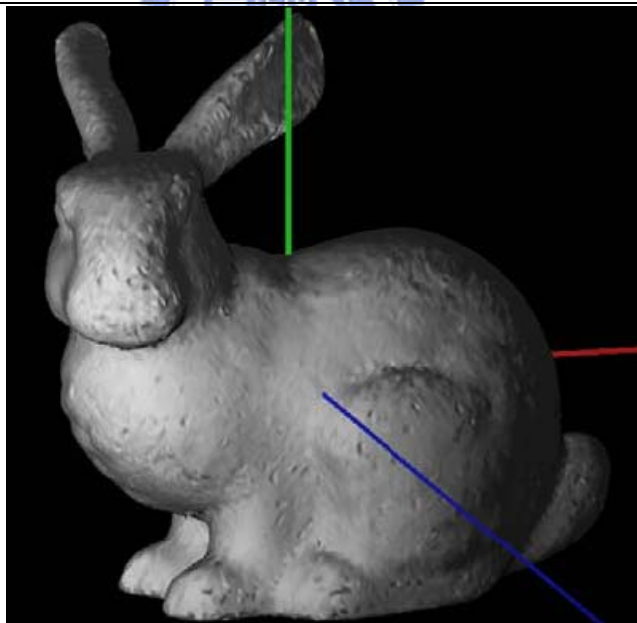
Optimization with – Phong Model

Phase 1-Diffuse Optimization



Cost Error Initial: 9.000712 per pixel Current: 0.019035 per pixel
Reflectance parameters: $k_d=1.236784$

(a) Reflectance

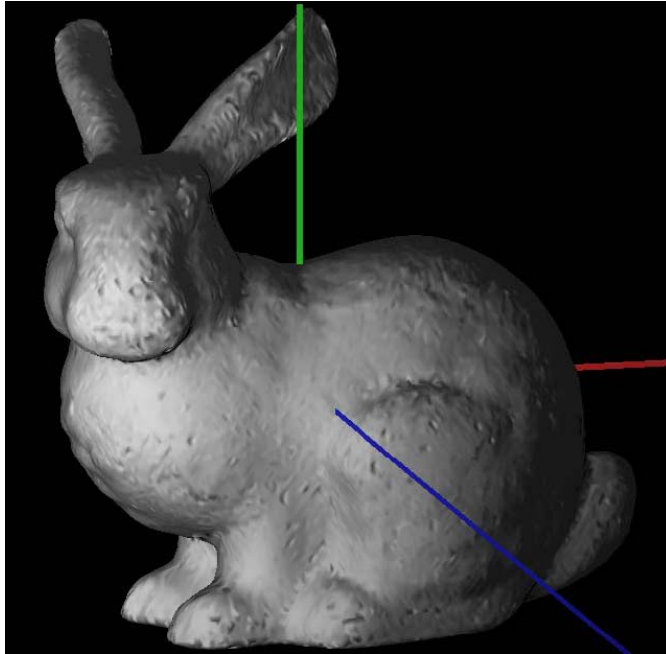


initial position cost error=42.584771 per pixel
last position cost error=38.288401 per pixel
smooth weight = 0.1

(b) Positions

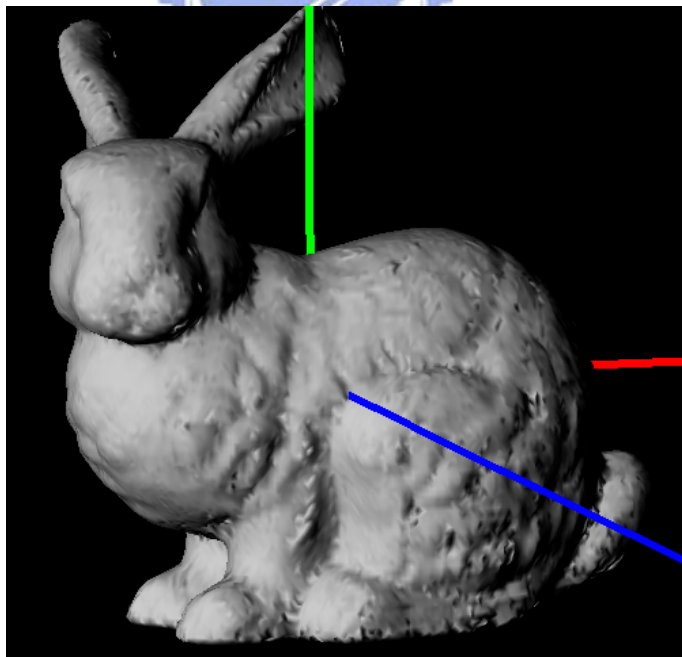
Fig.24 Phase 1 Optimization

Phase 2 – Specular Optimization



Cost Error Initial: 0.019035 per pixel Current: 0.003346 per pixel
Reflectance parameters: $k_d=0.779817, k_s=0.177215, \text{shininess}=0.598451$

(a) Reflectance

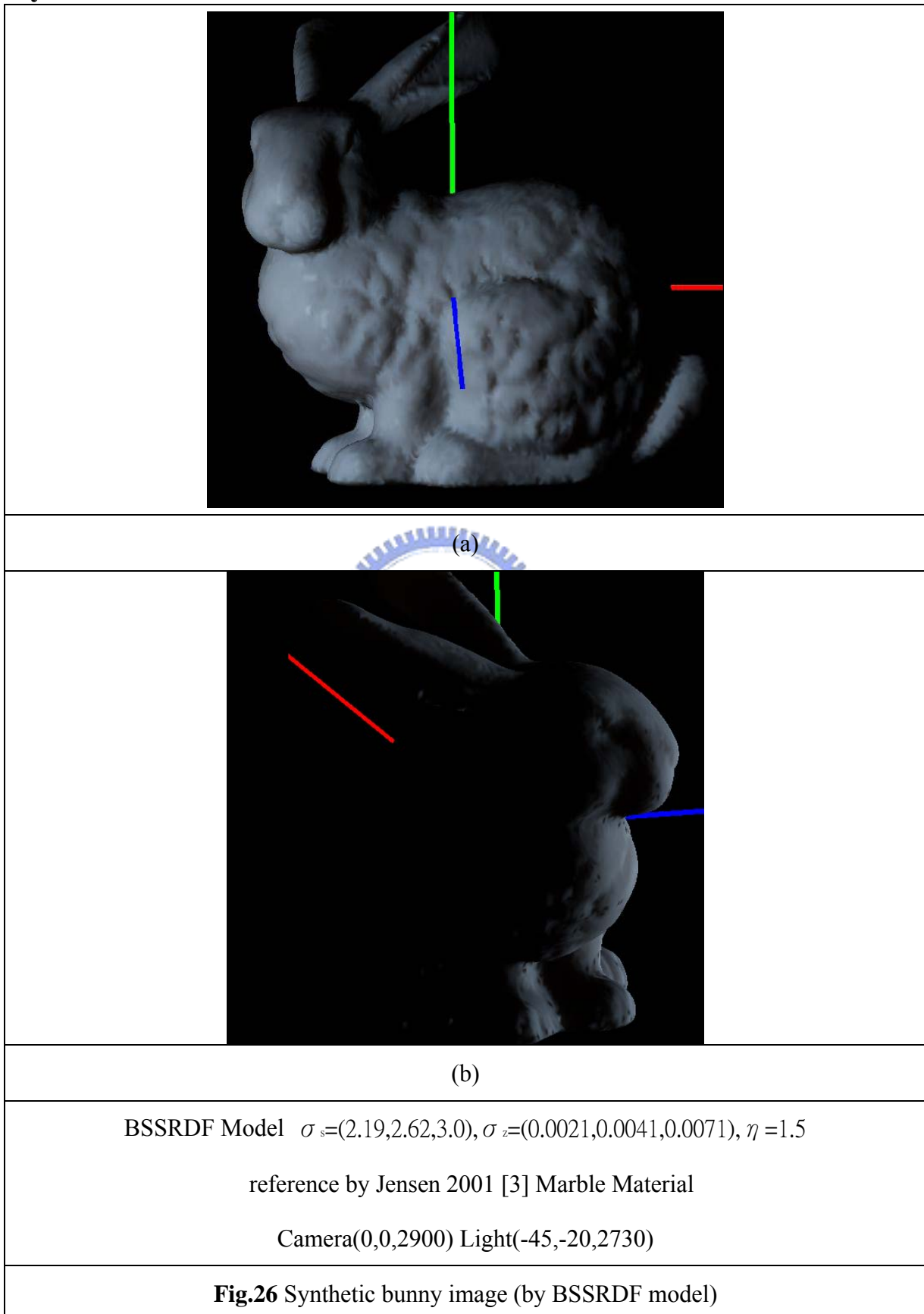


initial position cost error=3.5548330 per pixel
last position cost error=3.4629534 per pixel

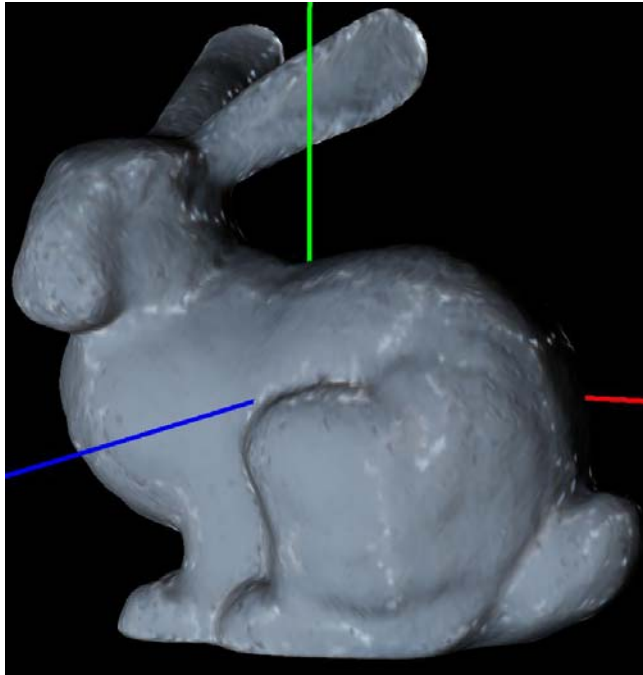
(b) Positions

Fig.25 Round 2 reflectance optimized data

Optimization with – BSSRDF Model Synthesis Reflectanc

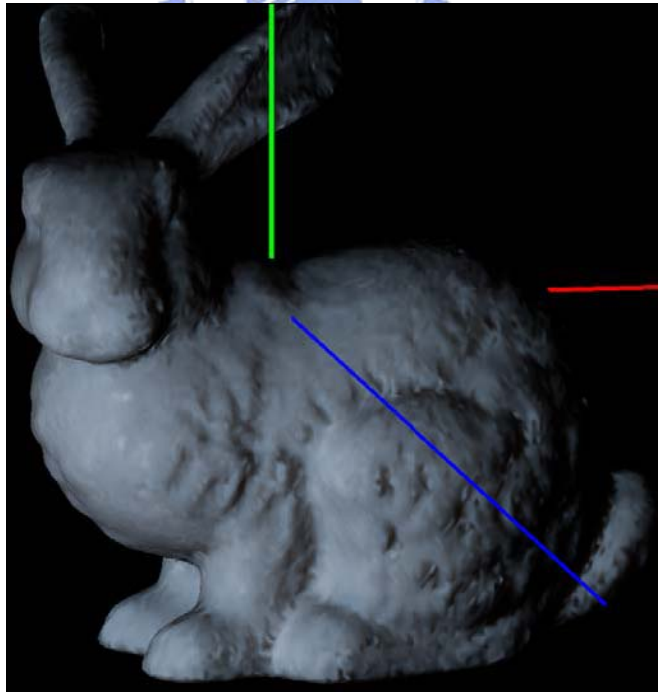


Optimize Synthesis-BSSRDF model



cost error = 0.32 per point

(a) Phase 1



final cost error = 0.29 per point

(b) Phase 2

Fig.27 Result position optimized data

5.2 A marble statue

5.2.1 Stereo positions

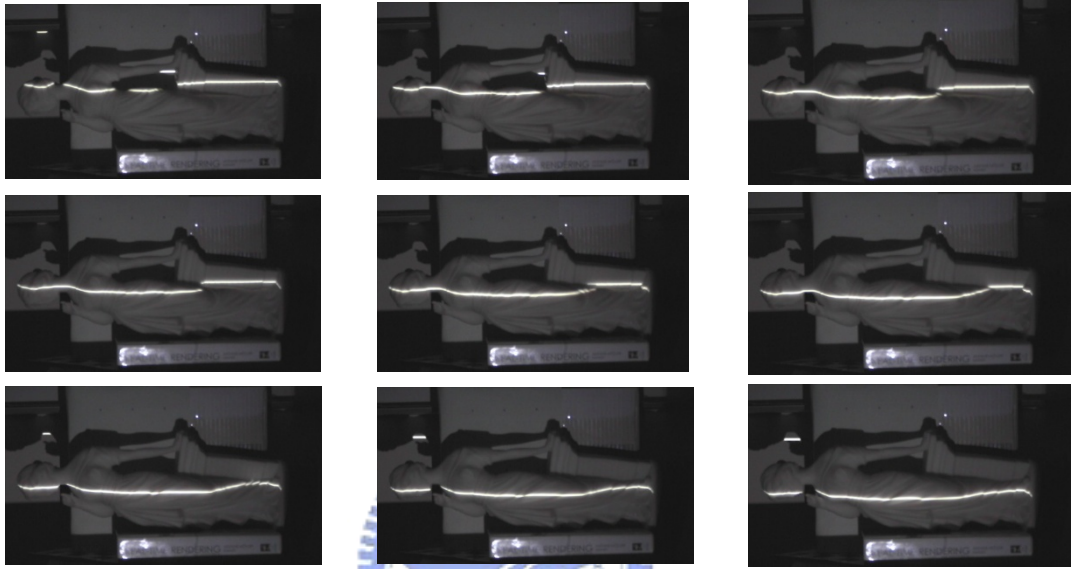
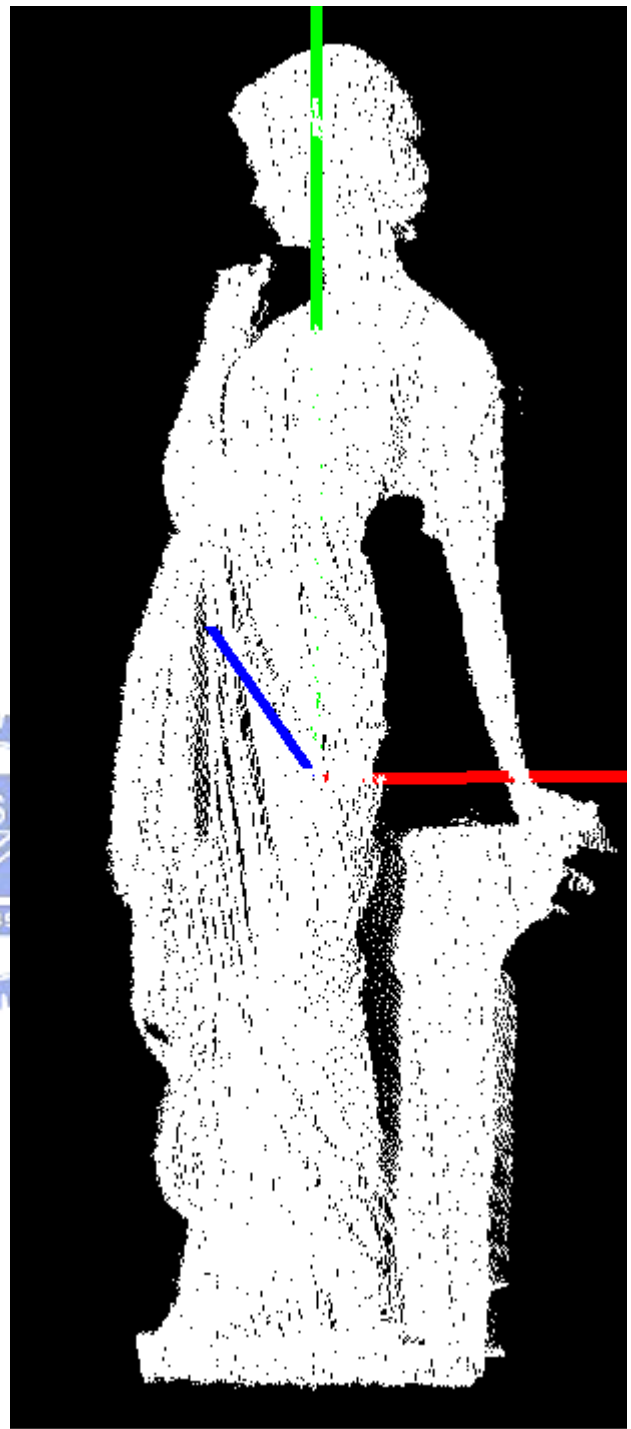


Fig.28 Input structured light images.

Table2

data information	
Vertex number	81,027

Reconstruction Result



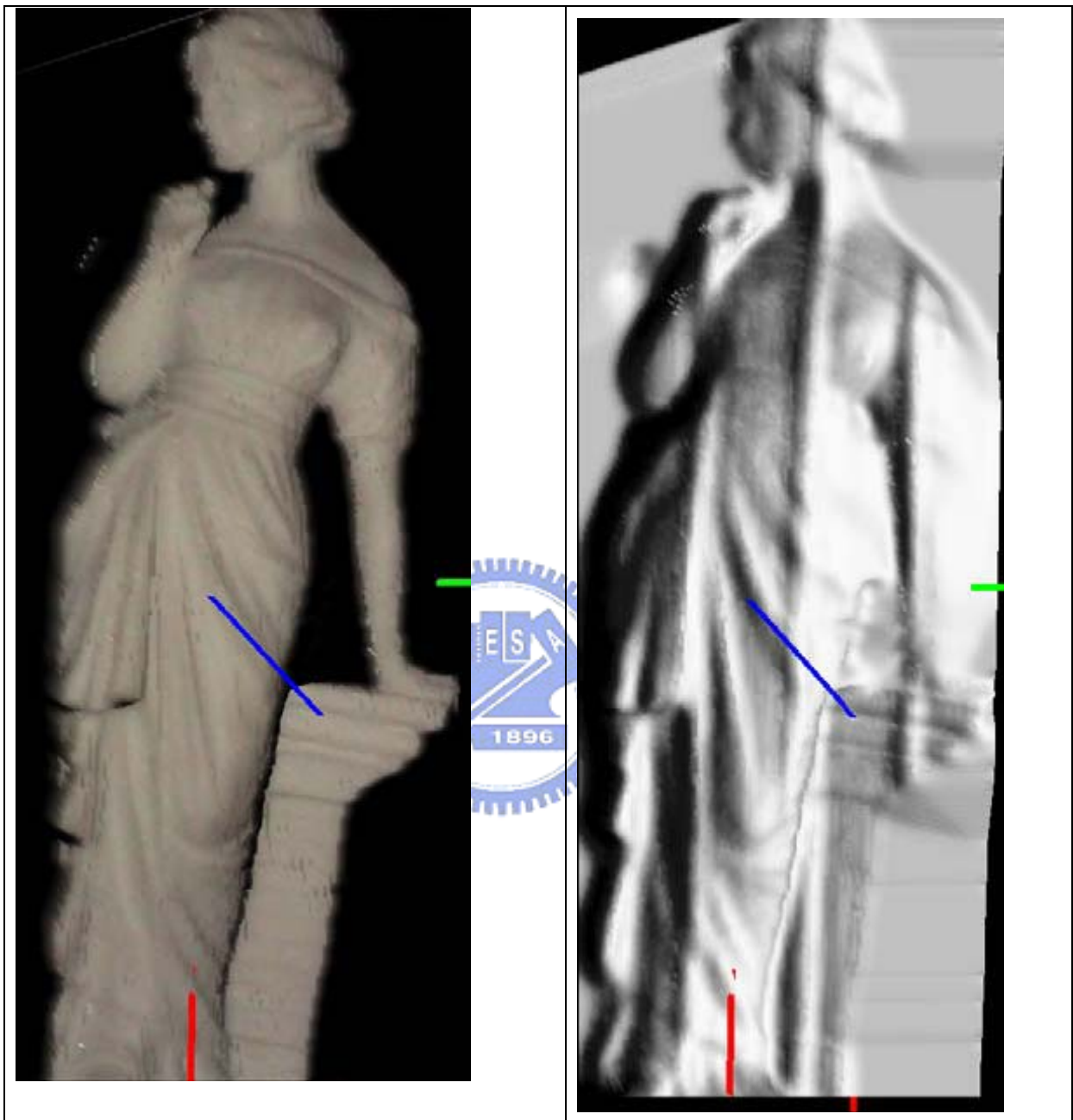
(a)

(b)

Fig.29 (a)an input reflectance image (b) scanned data

5.2.2 Optimized Result

Optimization with Phong reflection model



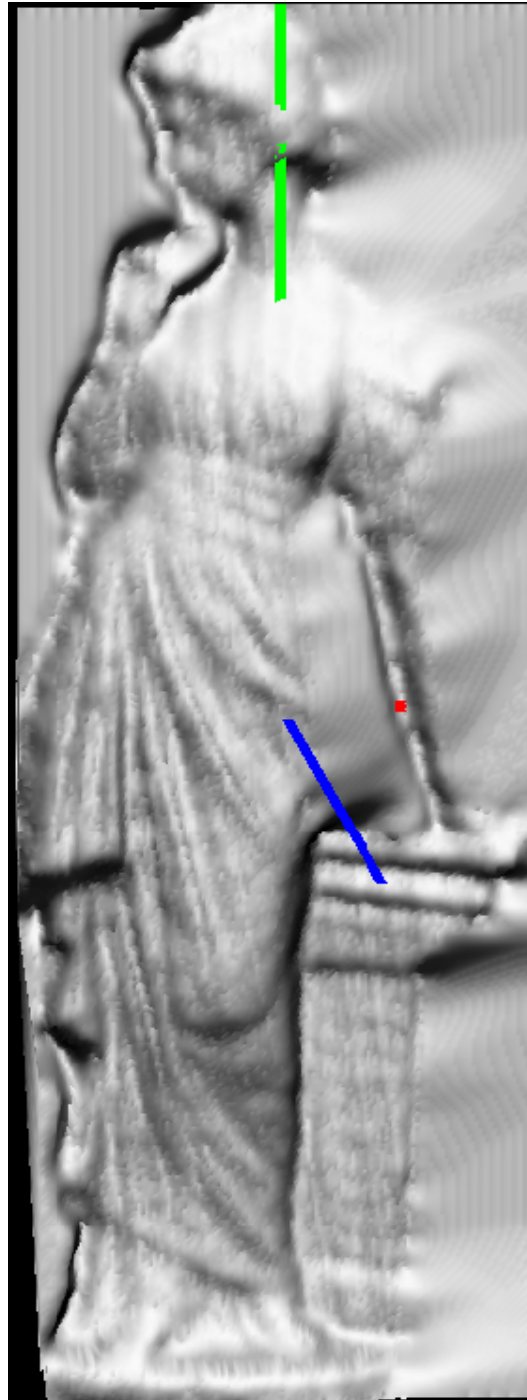
Reflectance parameters:

Initial: $k_d=0.8$, $k_s=0.2$, $\alpha=0.5$, error= 0.127580 per-point

Optimize: $k_d=0.6428$, $k_s=-0.164$, $\alpha=4.41$, error= 0.006225 per-point

Fig.30 The left image shows real reflectance color, and the right image shows optimized reflectance color

Phong Position Optimization



Position error:

Initial: 0.261 per point

Optimizing: 0.258 per point

Fig.31 The result of Phong optimized position

Chapter 6. Conclusion and Future work

6.1 Conclusion

This thesis proposes a reconstruction approach that makes use of the reflectance properties to optimize both the stereo positions and the reflectance parameters. The Phong and the BSSRDF model are used as our reflectance model. Therefore, the details of non-lambertian and the sub-surface scattering objects can be reconstructed by our approach. There are three stages in our approach: First, we utilize the projective calibration to reconstruct a 3D stereo position. Then, the Phong and the BSSRDF reflectance model are used to estimate the reflectance parameters. Last, the estimated reflectance parameters are further utilized to optimize the stereo positions. Our contributions are as follows:

- (d) Improving the scanning accuracy of non-lambertian and sub-surface scattering objects.
- (e) Utilizing only inexpensive devices.
- (f) The reflectance parameters are also estimated. We can use them to render the object from different views and lighting conditions.

6.2 Future work

Our system can be further improved from the following aspects. Our stereo structured light system is not accurate enough but easy to implement. The accurate 3D scanner can be applied for more accurate initial guesses. The BSSRDF reflectance model that we utilize requires heavy computation. Therefore, we only use it for partial detail improvement. Recently, many simplified BSSRDF models are proposed, these reflectance models may also be integrated in to our approach.

Reference

- [1] D. Nehab, S. Rusinkiewicz, J. Davis, R. Ramamoorthi, "Efficiently Combining Positions and Normals for Precise 3D Geometry.", Proceedings of ACM SIGGRAPH, pp. 536 – 543, 2005.
- [2] T. Yu, N. Xu, N. Ahuja, "Recovering Shape and Reflectance Model of Non-Lambertian Objects from Multiple Views," CVPR, pp. 226-233, 2004.
- [3] H. Jensen, S. Marschner, M. Levoy, and P. Hanrahan, "A Practical Model for Subsurface Light Transport", Proceedings of SIGGRAPH, pages 511-518, 2001.
- [4] D. Huynh, "Calibration of a Structured Light System: A Projective Approach", CVPR, Page: 225, 1997.
- [5] C. H. Chen and A. C. Kak. "Modeling and Calibration of a Structured Light Scanner for 3-D Robot Vision". In Proc. IEEE Conf. Robotics and Automation, volume 2, pp. 807-815, 1987.
- [6] L. Zhang, B. Curless, and S. M. Seitz. "Spacetime Stereo: Shape Recovery for Dynamic Scenes". In Proceedings of IEEE Computer Society Conference on Computer Vision and Pattern Recognition (CVPR), Madison, W, pp. 367-374, I, June, 2003
- [7] A. Hertzmann, S. M. Seitz. "Shape and Materials by Example: A Photometric Stereo Approach". Proc. IEEE CVPR 2003. Madison, WI. June 2003. Vol. 1. pp. 533-540, 2003.
- [8] H. Fang and J. C. Hart. "Textureshop: Texture Synthesis as a Photograph Editing Tool." Proc. SIGGRAPH, 2004.
- [9] F. E. Nicodemus, J. C. Richmond, J. J. Hsia, I. W. Ginsberg, and T. "Limperis. Geometric considerations and nomenclature for reflectance". Monograph 161, National Bureau of Standards (US), October 1977.
- [10] C. Donner and H. W. Jensen, "A Spectral BSSRDF for Shading Human Skin"

Eurographics Symposium on Rendering, pages 409-417, ACM Transactions on Graphics (SIGGRAPH'2005), pp. 1032-1039, 2005.

[11] K. M. Lee, C. J. Kuo, "Shape from Shading with a Generalized Reflectance Map Model", Computer vision and image understanding, Vol. 67, No. 2, pp. 143–160, Aug. 1997.

[12] A. Hertzmann, S. Seitz, "Shape and Materials by Example: A Photometric Stereo Approach", Computer Vision and Pattern Recognition, 2003. Proceedings. Vol. 1, pp. 533-540, June 2003

[13] G. Vogiatzis, P. H. S. Torr, R., " Volumetric graph-cut", Cipolla, Proceedings of the 2005 IEEE Computer Society Conference on Computer Vision and Pattern Recognition (CVPR'05) , 2005.

[14] S.R. Marschner, "Inverse Rendering for Computer Graphics," Ph.D. Thesis, Cornell University, Aug. 1998.

[15] P. Debevec, T. Hawkins, C. Tchou, H.P. Duiker, W. Sarokin, and M. Sagar. "Acquiring the reflectance field of a human face", Proceedings of the 27th annual conference on Computer graphics and interactive techniques, pp. 145– 156. 2000

[16] R.C. Love. "Surface Reflection Model Estimation from Naturally Illuminated Image Sequences", PhD thesis, The University of Leeds, Sep. 1997.

[17] J. I. Apricio, J.G.Garcia-Bermejo, "An Approach for Determining Phong Reflectance Parameters from Real Objects," Pattern Recognition, 2000. Proceedings. 15th International Conference on, pp. 568 -571 vol.3 Sept. 2000

[18] R. Ramamoorthi and P. Hanrahan, "A Signal-Processing Framework for Inverse Rendering", Proceedings of the 28th annual conference on Computer graphics and interactive techniques, pp.117-128, 2001

[19] Y. Sato, M. D. Wheeler, and K. Ikeuchi. "Object shape and reflectance modeling from observation", Proceedings of the 24th annual conference on Computer graphics and interactive techniques, pp. 379–388, 1997.